https://doi.org/10.5194/egusphere-2026-5508
Preprint. Discussion started: 29 September 2026

Assessing VIIRS aerosol data assimilation as a MODIS successor in the NASA GEOS system

Virginie Buchard[1,2], Patricia Castellanos[2], Arlindo M. da Silva[2,3,4], Ravi Govindaraju[5,2], Matthew A. Thompson[5,2], Rob Levy[6], Jaehwa Lee[6,7], Vincent Kim[8,9], Pawan Gupta[10]

[1]Goddard Earth Sciences Technology and Research II (GESTAR II), University of Maryland Baltimore County, Baltimore, Maryland, USA
[2]Global Modeling and Assimilation Office, NASA Goddard Space Flight Center, Greenbelt, Maryland, USA
[3]Center for Research on Sustainable Forests, University of Maine, Orono, Maine, USA
[4]Asticou Earth Systems LLC, Bar Harbor, Maine, USA
[5]Science Systems and Applications, Inc., Lanham, Maryland, USA
[6]Climate and Radiation Laboratory, NASA Goddard Space Flight Center, Greenbelt, Maryland, USA
[7]Earth System Science Interdisciplinary Center, University of Maryland, College Park, Maryland, USA
[8]Entarian, Greenbelt, Maryland, USA
[9]NOAA Weather Prediction Center - Extended Prediction Division, College Park, MD, USA
[10]Biospheric Science Laboratory, NASA Goddard Space Flight Center, Greenbelt, Maryland, USA

Correspondence to: Virginie Buchard (virginie.buchard@nasa.gov)

Abstract. Aerosol data assimilation is critical for global Earth system modelling, improving aerosol optical depth (AOD) representation for weather and atmospheric composition forecasts and reanalyses. For two decades, MODIS sensors on Terra and Aqua were the primary observation source for operational aerosol assimilation within the NASA Goddard Earth Observing System (GEOS). As MODIS nears decommission, VIIRS aboard NOAA satellites represent its successor. This transition trades the MODIS morning satellite for VIIRS's increased data volume, gapless equatorial coverage, and finer spatial resolution. This study assesses the assimilation of VIIRS NOAA-20 AOD within GEOS.

To ensure observing platform consistency, GEOS uses a Neural Network Retrieval (NNR) algorithm translating radiances into AERONET-calibrated AOD, homogenizing MODIS and VIIRS observations before assimilation. Two experiments (March 2019–February 2020) compared a control assimilating NNR MODIS Terra/Aqua against a test assimilating NNR VIIRS NOAA-20.

Validation against AERONET and Maritime Aerosol Network observations shows that, despite lacking a morning satellite, VIIRS alone performs competitively with combined MODIS, with comparable correlations and error metrics. Relative performance varies by aerosol regime. In dust-dominated environments, VIIRS frequently yields better agreement with AERONET due to finer resolution and greater data volume. During biomass burning, MODIS shows a slight advantage from stronger diurnal constraints on rapidly varying smoke plumes. Both experiments underestimate peak AOD during wildfires (stemming from the ~50 km grid artificially diluting concentrated smoke) and in African mixed-aerosol highlands (driven by

https://doi.org/10.5194/egusphere-2026-5508
Preprint. Discussion started: 29 September 2026

topographic smoothing). Overall, VIIRS observational density compensates for reduced temporal sampling, supporting a reliable transition for GEOS aerosol forecasting and reanalyses.

1 Introduction

Aerosols have a significant impact on the Earth system through direct and indirect radiative effects. The spatio-temporal distribution of aerosols and their properties are crucial to representing fundamental Earth System processes in global circulation models. Consequently, aerosols and their radiative interactions have been incorporated into many Earth system models over the years (Kinne et al., 2006; Kaiser et al., 2019; Wang et al., 2020), and increasingly aerosols are a component of global weather and air quality forecasting systems (Benedetti et al., 2018; Xian et al., 2019; Lynch et al., 2016), as well as multi-decadal reanalyses (Inness et al., 2019). Two such implementations are the NASA Goddard Earth Observing System Forward Processing (GEOS-FP) system (Lucchesi, 2018), which provides near-real time aerosol assimilation and forecasting to support NASA missions, and the Modern-Era Retrospective Analysis for Research and Applications, version 2 (MERRA-2) (Randles et al., 2017, Buchard et al. 2017), which was the first global multi-decadal reanalysis wherein meteorological and aerosol observations were jointly assimilated. Both global modelling and analysis systems are based on the GEOS global circulation model coupled to the GOCART (Goddard Chemistry, Aerosol, Radiation, and Transport model) aerosol module (Chin et al., 2000). The aerosol analyses and predictions based on GEOS have numerous applications such as field mission support and planning, serving as *a priori* profiles for satellite retrievals of other atmospheric constituents, ecosystem monitoring, and tracking extreme events.

Data assimilation of aerosol properties such as aerosol optical depth (AOD) has emerged as a powerful technique to improve aerosol representation in global models by systematically combining satellite observations with numerical model forecasts. This approach combines modelling with observational data to produce a most probable representation of the four-dimensional distribution of aerosols. While aerosol observations by polar orbiting satellites may be somewhat sparse lacking detailed vertical information, irregularly spaced both spatially and temporally, and representative of only a limited spatial and temporal scale, a model simulation provides a continuous and physically consistent representation of the integrated Earth system. In turn, the assimilation of aerosol observations can correct biases in the model simulations and reposition plumes arising from erroneous transport. AOD data assimilation has been shown to provide better agreement with independent observations such as surface PM2.5 (Bocquet et al., 2015; Buchard et al., 2016), satellite-based estimates of aerosol index (Buchard et al., 2015), and vertical profiles of attenuated backscatter (Buchard et al., 2017). Through on-line radiative coupling, aerosol data assimilation can also impact atmospheric dynamics, and AOD assimilation has been shown to improve weather forecasts (Pérez et al., 2006; Mulcahy et al., 2014; Wei et al., 2021).

https://doi.org/10.5194/egusphere-2026-5508
Preprint. Discussion started: 29 September 2026

Data assimilation also serves to synthesize the observations from various platforms that make up the Earth observing system. Over the years many instruments have had capabilities to measure aerosol properties, and various algorithms have been developed to retrieve AOD from the measurements. This has led to a number of independent datasets of AOD observations with different resolutions, biases and uncertainties. For example, for the MERRA-2 multi-decadal reanalysis, AOD observations from five different observing platforms were assimilated. From the year 2000 onward the Moderate Resolution Imaging Spectroradiometer (MODIS) instrument has been the source of the vast majority of AOD observations assimilated in both GEOS-FP and MERRA-2, as well as many other aerosol assimilation systems (Xian et al., 2019). Twin MODIS instruments fly on the Terra and Aqua satellites, over-passing the equator on the sunlit side of the earth at approximately 10:30 and 13:30 local solar time, respectively. The ground-based Aerosol Robotic Network (AERONET) provides another key set of AOD observations that are widely assimilated. This globally distributed network of surface observations provides day and night high frequency (every 5 to 15 minutes), low uncertainty estimates of AOD.

However, with Terra launched in 1999 and Aqua in 2002, the MODIS observations will soon be discontinued, raising concerns about long-term data continuity for operational aerosol monitoring systems. The Visible Infrared Imaging Radiometer Suite (VIIRS) aboard NOAA's polar-orbiting satellites represent the next generation of operational aerosol monitoring capability. VIIRS was designed to continue many of MODIS's measurement capabilities while providing enhanced spatial resolution and improved calibration stability, making it a natural successor for operational aerosol data assimilation. There are currently three VIIRS sensors in orbit.

When the various AOD datasets are assimilated, any biases in the data can propagate in the model simulation and lead to artificial spatial and temporal variability. Zhang and Reid (2006) and Lary et al. (2009) showed that systematic biases in the MODIS AOD data record with respect of AERONET AOD are linked to surface reflectance, solar and viewing geometry, and cloud cover metrics. To address this in the MERRA-2 reanalysis, an algorithm was developed, referred to as the neural network retrieval (NNR), that homogenizes the observing system by means of a neural network scheme that translates satellite observed top-of-the-atmosphere (TOA) reflectance into AERONET observed AOD (Randles et al., 2017). In this system, MODIS TOA reflectance provides the main input, alongside solar and viewing geometry, MODIS cloud cover, climatological surface albedo and model-derived surface wind speed. Saide et al. (2013) evaluated the NNR AOD against other observational datasets using the WRF-Chem data assimilation system and showed a reduced bias in the assimilation relative to independent observations.

This paper presents the implementation of the NNR algorithm to VIIRS AOD data products that will provide the foundation for future GEOS-based aerosol near-real time forecasting and reanalysis products. In the following sections, we describe the overall approach to developing the NNR, the specific datasets used, and the testing and validation of the neural network predicted AOD. Furthermore, this study comprehensively assesses the performance of VIIRS AOD assimilation within the GEOS aerosol assimilation system for the period of 2019 through early 2020. We compare two parallel experiments: a control

https://doi.org/10.5194/egusphere-2026-5508
Preprint. Discussion started: 29 September 2026

simulation assimilating MODIS Terra and Aqua NNR AOD products at 550 nm, and a test simulation assimilating VIIRS NOAA-20 NNR AOD products at the same wavelength. Through detailed analysis of assimilation statistics, independent validation against AERONET observations, and examination of regional and seasonal performance variations, we assess the impact of transitioning from MODIS to VIIRS for NASA's operational aerosol analysis and forecasting systems. This evaluation is critical for ensuring continuity of high-quality aerosol products as the satellite observing system transitions from MODIS to VIIRS in the coming years.

2 Methodology

2.1 GEOS Model System

2.1.1 Aerosols in GEOS

The Goddard Earth Observing System (GEOS), developed by NASA's Global Modelling and Assimilation Office (GMAO), is a comprehensive Earth system model that incorporates atmospheric circulation and composition, ocean circulation and biogeochemistry, and land surface processes. Aerosols in GEOS are simulated using the GOCART module, recently refactored as GOCART Second Generation (GOCART-2G, Collow et al., 2023) enhancing performance, flexibility, and code quality for operational and research applications. The model maintains the proven bulk aerosol approach that balances computational efficiency with scientific accuracy, making it suitable for near-real-time operational forecasting while avoiding the computational expense of more complex sectional or modal schemes.

GOCART-2G simulates seven radiatively active aerosol species treated as externally mixed components: dust, sea salt, organic carbon (OC), brown carbon (BrC), black carbon (BC), sulfate (SO4), and nitrate. Dust and sea salt have wind-speed dependent emissions and are each represented by five non-interacting size bins, following the MERRA-2 approach. Regarding the carbonaceous aerosols, the model now distinguishes between organic carbon, brown carbon that is emitted mainly by biomass burning, and black carbon, with each having both hydrophobic and hydrophilic components. Sulfate is represented as a single tracer. Primary sulfate and carbonaceous aerosol emissions come principally from fossil fuel combustion, biomass burning, and biofuel consumption, with additional biogenic sources of organic carbon. Secondary sources of sulfate include chemical oxidation of sulfur dioxide gas (SO2) and dimethyl sulfide (DMS), with a database of volcanic SO2 emissions and injection heights also included. Nitrate is incorporated using three size bins (one fine-mode and two coarse-mode) and secondary nitrate formation is based on thermodynamic equilibrium processes.

Loss processes for all aerosols include dry deposition (including gravitational settling), large-scale wet removal, and convective scavenging, with additional sedimentation for dust and sea salt. Aerosol optical properties are calculated using lookup tables derived from Mie theory, with species-specific treatments for non-spherical dust particles and hygroscopic

https://doi.org/10.5194/egusphere-2026-5508
Preprint. Discussion started: 29 September 2026

growth that depends on simulated relative humidity (Colarco et al., 2010). Hygroscopic effects are considered in computations of particle fall velocity, deposition velocity, and optical parameters.

Numerous studies have demonstrated the skill of the GOCART aerosol module in simulating AOD and other observable aerosol properties (e.g., Colarco et al. 2010; Nowottnick et al. 2010, 2011; Bian et al. 2013, Buchard et al., 2015, 2016, 2017; Randles et al., 2017). Further details on GOCART-2G, including the aerosol optical properties used, are in Randles et al. (2017) and Collow et al. (2023).

2.1.2 GEOS Aerosol Assimilation System (GAAS): Analysis splitting approach

The GEOS aerosol data assimilation system employs the Goddard Aerosol Assimilation System (GAAS) to assimilate AOD observations at 550 nm from various platforms into the GEOS-GOCART-2G modelling system. This system has been successfully implemented in both the near-real-time GEOS Forward Processing (GEOS-FP) system, the MERRA-2 reanalysis (Randles et al., 2017), GEOS-IT (an analysis product for instrument teams) and is used in the next reanalysis MERRA-21C.

Every three hours, the aerosol assimilation is performed using an analysis splitting approach that operates in two distinct steps. First, a two-dimensional (2D) AOD analysis is conducted by combining short-term model forecasts with quality-controlled observations using a 2D version of the Physical-Space Statistical Analysis System (PSAS; Cohn et al. 1998). To address the non-Gaussian distribution of AOD values, the analysis is performed using a log-transformed control variable ($X = \ln(AOD + \varepsilon)$, where $\varepsilon = 0.01$), which provides more appropriate error characteristics for both small and large AOD values.

The analysis represents the best estimate of AOD at any given time. Since GOCART simulates three-dimensional aerosol mass mixing ratios as prognostic variables, the second step translates the two-dimensional AOD increments into corresponding three-dimensional mass concentration increments for each aerosol species. This is accomplished using the Local Displacement Ensemble (LDE) methodology, which considers aerosol properties in neighbouring grid boxes to estimate an ensemble of vertical aerosol profiles which in turn are used to parameterize the background error covariance structure and vertically distribute AOD increments. While single-wavelength AOD assimilation effectively constrains the total aerosol column loading, it provides limited information about aerosol composition and vertical structure, which remains primarily determined by model parameterizations, the prescribed emissions and the inherent speciation implied by the LDE approach.

During the assimilation process, online quality control is implemented through an adaptive buddy check algorithm (Dee et al., 2001), with observation and background error statistics estimated using maximum likelihood methods (Dee and da Silva, 1999). The adaptive nature of this algorithm allows it to account for the spatial variability of surrounding observations, adjusting quality control thresholds based on the local observational density and consistency within neighbouring grid points. This approach enables more flexible rejection criteria in regions with high natural variability while maintaining stringent

https://doi.org/10.5194/egusphere-2026-5508
Preprint. Discussion started: 29 September 2026

quality control in areas with expected spatial homogeneity. To handle the substantially higher observation volumes from current and future satellite missions, the quality control algorithm has been parallelized using OpenMP for operational efficiency.

2.2 Aerosol Bias Correction via the Neural Network Retrieval (NNR) Approach

The overall approach for the development of the MODIS NNR algorithm as described in Randles et al. (2017) is as follows. A dataset of contemporaneous MODIS Terra and Aqua observations and AERONET AOD was created by averaging all AERONET observations within 30 min of a satellite overpass and all satellite observations within 27.5 km of an AERONET location. The satellite top of the atmosphere (TOA) multi-spectral reflectance observations are inputs to a back propagation neural network that predicts observed AERONET 550 nm AOD that has been log-transformed to be consistent with the GAAS approach described above. However, the retrieval of AOD from TOA reflectance is an indeterminate problem. The magnitude and spectral dependence of TOA reflectance is also impacted by the solar-sensor geometry, surface reflectance, cloud contamination, and the type of aerosol present in the observing scene. Note that the satellite TOA reflectance values utilized here are trace gas corrected (see below for details). Thus, ancillary data that provide *a priori* information about these aspects of the scene are also used as inputs to the neural network to constrain the relationship. Estimates of surface reflectance are provided by the satellite standard product assumptions, or in the case of ocean pixels the glint angle which is a proxy for ocean surface reflectance. The solar and sensor geometries are also inputs. Estimates of fractional AOD speciation are provided by the MERRA-2 reanalysis and by GEOS-FP during NRT inference. Finally, cloud contamination is screened for by enhanced quality control checks. The following provides details of all datasets used, quality control filtering and final data selection, as well as the extension of the NNR algorithm to VIIRS aerosol observations.

2.2.1 Datasets Used to Train the NNR

2.2.1.1 AERONET Observations

AERONET is a globally distributed network of automatic scanning radiometers that measure spectral direct sun & moon (pointing directly at the sun and moon in the night) and sky radiance (almucantar and principal plane radiance measurements). Several versions of these radiometers have been in use since the inception of AERONET in 1993 (Holben et al., 1998), but the most basic sensor includes 8 filters at 1020, 936, 870, 675, 500, 440, 380, and 340 nm. Since 2004, most sensors have been replaced with upgraded versions adding polarization, additional wavelengths (e.g. 1640 nm), and improved tracking and robot control (https://aeronet.gsfc.nasa.gov/new_web/system_descriptions_instrument.html). Since 2014, the network has been upgraded with a new generation of sun photometers (Cimel C318-T) that offer enhanced capability for nighttime aerosol measurements.

https://doi.org/10.5194/egusphere-2026-5508
Preprint. Discussion started: 29 September 2026

From the direct sun measurements, taken every 5 to 15 min, total column AOD at each wavelength can be calculated with low uncertainty (±0.01-0.021; (Eck et al., 1999)), which is primarily due to calibration uncertainty that is air mass and spectrally dependent with the higher errors in the UV. The latest version (Version 3) of the AERONET data record used in this study includes improved calibration and quality control (Giles et al., 2020).

AERONET sites are located worldwide on all continents and some oceanic islands (approximately 570 active sites in 2026, in total 618 sites were used for this study), but the availability of observations from individual sites varies throughout the data record. AERONET version 3 Level 2 (quality controlled and cloud cleared) data were used for this work. AOD values at 550 nm were used as the targets for the neural network and, when unavailable, was interpolated using the Angström relationship and adjacent AOD channels.

2.2.1.2 MODIS Terra/Aqua Satellite Observations

The twin MODIS instruments have provided global quantitative and systematic measurements of backscattered spectral radiance from the visible to thermal infrared since their launches in 1999 (onboard Terra) and 2002 (onboard Aqua) (Salomonson et al., 1998). Their broad spectral range, wide swath (2330 km), near daily global coverage, and relatively fine spatial resolution (1 km or less at nadir) make MODIS observations favourable for retrieving bulk aerosol properties (Kaufman and Tanre, 1996) and assimilation into global earth system models.

MODIS aerosol retrieval algorithms take advantage of observed wavelength bands that are in “window” channels where trace gas absorption is minimal or can be accurately estimated. The measured reflectance at the top-of-atmosphere (TOA) in these channels will contain contributions from aerosols, as well as molecular scattering, Earth’s surface, and clouds. Using selected assumptions, the goal is to isolate the aerosol signal. Over the years, many customized algorithms and techniques, often optimized to a specific location or condition, have been developed to retrieve AOD from MODIS observations. Here we consider three that are global, provide near-real time products, span the MODIS data record, and have been extensively documented and validated in the literature. Two are so-called 'Dark Target' algorithms, one is for over ocean (DT-Ocean) and one is for over visibly dark land surfaces (DT-Land) (Levy et al., 2013). The third is the so-called 'Deep Blue' algorithm that extends MODIS aerosol retrievals to over arid (visibly bright) surfaces (DB-Deep) (Sayer et al., 2014). The Deep Blue algorithm also retrieves AOD over ocean and dark land surfaces but differs from the traditional dark target algorithm by having alternative cloud mask and treatment of the surface reflectance. As each algorithm has been optimized for different combinations of aerosol types, surfaces, and cloud conditions, they each make different assumptions and have strengths and weaknesses.

MODIS has 36 wavelength bands spanning from 410 to 14400 nm with nominal resolutions of 250 m, 500 m or 1 km at nadir. The combination of the DT and DB aerosol retrieval algorithms make use of nine “windows” channels between 412 and 2130

https://doi.org/10.5194/egusphere-2026-5508
Preprint. Discussion started: 29 September 2026

nm to retrieve aerosol characteristics, along with other near-infrared and infrared bands to screen observations that are cloudy or contain ice or snow. Each of the three algorithms use subsets of these bands. The concept behind the Dark-Target algorithms is to observe over "dark" surfaces that have low reflectance in the visible bands. DT-Land estimates the surface contribution to the TOA reflectance by using observations at 2130 nm, where atmospheric scattering contributions are small. For primarily vegetated and dark-soiled surfaces where the scene appears sufficiently dark, this 2130 nm surface reflectance is used to estimate surface reflectance at visible wavelengths (470 nm and 660 nm) via an assumed spectral and directional relationship. For DT-Ocean, the surface reflectance is estimated as a function of windspeed and observing geometries. Thus, both DT algorithms can take advantage of the contrast between light scattering (bright) aerosols over surfaces that appear dark (vegetated land and oceans). The Deep Blue algorithm shares many characteristics of the Dark Target algorithms, in that it takes advantage of scenes that offer contrast between the aerosol and surface below. However, the Deep Blue algorithm also uses the deep blue channel (e.g. 412 nm) as well as an *a priori* global database to prescribe directional surface reflectance characteristics. Thus, Deep Blue can retrieve aerosols over dark surfaces as well as visually bright arid surfaces that appear dark in the 412 nm deep blue band.

Regardless of the approach, both algorithms start by taking calibrated MODIS reflectances (in their selected window bands), and correcting for the absorptions of water vapor, ozone, and other trace gases (e.g. Levy et al., 2013). Native-resolution pixels are aggregated to NxN boxes, which for the standard DT and DB products represents nominal 10 km x 10 km areas (at nadir). Each algorithm then makes its own choices for screening pixels that represent clouds, surface glint, and/or other unsuitable aerosol retrieval conditions, leaving a subset of pixels to be used in the retrieval within the box. For the Dark Target retrievals, additionally the brightest 25% and darkest 25% of remaining pixels over ocean, and the brightest 50% and darkest 20% over land are discarded. The remaining pixels, therefore, represent "suitable" conditions for aerosol retrieval, which may represent only a fraction of the 10 km x 10 km box area. In the case of Dark Target, the values in each wavelength are averaged to give a spectral reflectance that theoretically represents the gas-corrected, clear-sky (non-cloud, non-bright, non-ice/snow, etc.), reflectance in the box. Assuming there are enough remaining pixels in that box, the Dark Target algorithm makes a single aerosol retrieval to represent that box. Quality assurance/confidence of that retrieval is in part based on the fraction of pixels remaining to make a retrieval – higher confidence requires more remaining pixels. Although performing on the same 10 km x 10 km area box, the Deep Blue algorithm follows a different logic. After performing its own screening/masking logic, there is no further screening of remaining brightest and darkest pixels. In addition, DB makes aerosol retrievals from each of the remaining pixels, and those results are averaged to provide a final aerosol retrieval. DB follows its own choices for assigning confidence and quality assurance to retrievals. This means that for the same 10 km x 10 km over-land boxes, Deep Blue and Dark Target could be operating on very different subsets of the NxN native-resolution pixels.

The 10 km TOA trace-gas corrected reflectance values representing clear-sky conditions for the three retrieval algorithms are reported in the MODIS aerosol data products called MOD04 for Terra, and MYD04 for Aqua. For Dark Target, they are

https://doi.org/10.5194/egusphere-2026-5508
Preprint. Discussion started: 29 September 2026

reported at the used wavelengths of 0.47, 0.55, 0.65, 0.86, 1.24, 1.63, and 2.11 μm, and while not used, are also reported at 0.412, and 0.443 μm. The Deep Blue algorithm reports TOA reflectance at only 0.412, 0.47, and 0.65 μm. Note that three sets of these reflectance values are reported in the MOD04 and MYD04 data files - one each for the Dark Target Land, Dark Target Ocean, and Deep Blue retrievals. Note the overlap of wavelengths between DT-Land and DB-Land, but their values will likely be different due to different pixel selection choices described above. The AOD neural network retrieval takes advantage of the extensive cloud screening, quality control and trace gas corrections implemented by the Dark Target and Deep Blue algorithms by using the MOD04 and MYD04 reported 10 km TOA reflectance values as inputs to the neural network.

Here, the TOA reflectances reported within the collection 6.1 version of the MODIS data record was used in this study. The following quality control filters were applied to the MODIS observations prior to input to the NNR. First, the algorithm reported cloud fraction must be less than 0.70. For DT-Ocean we require that the glint angle is greater than 40°. For DT-Land and DB-Deep we require that the scattering angle is less than 170°. Finally, we use the reported quality assurance (QA) flags as follows. For DT-Land the QA flag must equal 3, and for DT-Ocean and Deep Blue the QA flag must be greater than 0.

2.2.1.3 VIIRS NOAA-20 Satellite Observations

The Dark Target and Deep Blue algorithms have been adapted with minor adjustments to the VIIRS satellites for continuity (Lee et al., 2024; Sawyer et al., 2025) providing similar data products and quality. Unlike MODIS, the VIIRS DT and DB products are generated as separate Level-2 datasets named AERDT and AERDB, respectively. The v2.0 of the AERDT and AERDB datasets are utilized in this study. Three VIIRS instruments are currently in orbit aboard Suomi-National Polar-orbiting Partnership (SNPP) and Joint Polar Satellite System-1 & 2 (JPSS-1 & 2: in operation as NOAA-20 & 21), and future launches are planned. As SNPP is scheduled to be decommissioned in 2026, the GEOS-FP system will transition its AOD assimilation to use VIIRS NOAA-20 observations. The similarity between the VIIRS and MODIS instruments makes continuity with MODIS possible, but differences in sampling, spatial resolution, spectral band responses, calibration, and the absence of some thermal infrared channels in VIIRS contributes to differences between AOD products (Sawyer et al., 2020).

Specifically, for the AERDT products, the algorithm approach was largely directly ported to VIIRS, also providing an over dark land surfaces and ocean AOD product (AERDT-Land and AERDT-Ocean, respectively). New look-up tables were generated for the specific bands of the VIIRS sensor as they deviate from MODIS slightly. Thus, the AERDT TOA reflectance is reported at 0.49, 0.55, 0.67, 0.87, 1.24, 1.60, 2.26 μm. Notably, the externally derived MODIS-VIIRS continuity cloud mask product used by the AERDT algorithm lacks one of the thermal infrared bands required for the cirrus test. The AERDB algorithm was expanded to include retrievals over ocean and dark land surfaces as well. However, these data were not used in the current study, only pixels that were determined to be bright land surface pixels by the algorithm (i.e. when 412 nm surface reflectance is reported) were used (AERDB-Deep). The AERDB-Deep retrieval reported TOA reflectance at 0.488, 0.67, and

https://doi.org/10.5194/egusphere-2026-5508
Preprint. Discussion started: 29 September 2026

2.25 µm. The AERDB algorithm utilizes an internal pixel suitability test to check for snow, ice, clouds, sun glint, and other invalid features and provides a suitable pixel fraction in lieu of a cloud fraction in their dataset. This quality screening feature was found to be insufficient for diagnosing possibly cloud contaminated pixels. Therefore, the AERDT cloud fraction (Aerosol_Cloud_Fraction_Land) was utilized as an additional screening metric for the AERDB product as described below. The MODIS and VIIRS spatial resolutions also differ, and thus the sub-pixel aggregation strategy does as well. Both the AERDT and AERDB algorithms utilize the VIIRS so-called M-bands with 0.75 km spatial resolution, and report AOD at 6 km resolution at nadir by aggregating 8x8 pixels either before retrieval at the radiance level (AERDT) or after retrieval (AERDB).

The three VIIRS AOD products were independently co-located with AERONET observations for the years 2019-2025. Given the ability of VIIRS to observe finer gradients in aerosol properties, the spatial colocation criterion for the ocean product was reduced to 15 km, but the temporal colocation remained within 30 min of satellite overpass. Similar quality control filters were applied to the AERDT and AERDB products as the MODIS AOD products. However, the AERDT reported cloud fraction must be less than 0.10 (rather than 0.70 utilized for MODIS). For AERDT-Ocean we require that the glint angle is greater than 40°. For AERDT-Land and AERDB-Deep products we require that the scattering angle is less than 170°. Finally, we use the reported quality assurance (QA) flags as follows: for AERDT-Land the QA flag must equal 3, and for AERDT-Ocean and AERDB, the QA flag must be greater than 0.

2.2.1.4 Model Speciated Aerosol

As detailed in Section 2.1.1, the GOCART module calculates total AOD as the sum of individual optical depths from the simulated aerosol species. We sampled the MERRA-2 reanalysis at the times and locations of the satellite-AERONET colocations and calculated the speciated AOD at 550 nm and found the relative contribution of each species to the total AOD. These speciated AOD fractions were used as inputs to the neural network as an a priori estimate of the aerosol type present in the scene, which impacts the magnitude of the TOA reflectance as well as the spectral dependence. It is notable that the NNR approach does not use a single aerosol type like typical aerosol retrieval algorithms, but instead prescribe a fractional AOD speciation.

2.2.2 Training and Validation of the VIIRS NNR for AOD

Tables 1-3 list the feature inputs used in the backpropagation neural networks that comprise the GEOS NNR for MODIS Terra and Aqua and VIIRS NOAA-20 (thus nine independent neural networks in total). Each neural network has a single hidden layer with 200 nodes with sigmoid activation function, and a single target which is log-transformed 550 nm AOD (X). Additional quality control was applied to the satellite-AERONET collocations prior to training. Only satellite-AERONET colocations for the years 2019-2024 were used for model development, with a subset reserved for testing, while the final year

https://doi.org/10.5194/egusphere-2026-5508
Preprint. Discussion started: 29 September 2026

2025 was held out entirely for independent validation. First, outlier removal was performed by removing pixels where the difference between the log-transformed AERONET AOD and the VIIRS standard AOD retrieval differed by greater than 3 standard deviations from the mean difference. This removes poorly representative observations (e.g. at the edge of the satellite swath, or the edge of a plume), or residual cloud contamination. Second, the dataset was balanced according to the GEOS predicted speciation. The dataset was down selected such that roughly equal numbers of points with dominant aerosol species occurred in the dataset. This promotes generalizability in the training.

MODIS	VIIRS
TOA reflectance at 0.412, 0.443, 0.47, 0.55, 0.65, 0.86, 1.24, 1.63, and 2.11 μm	TOA Reflectance at 0.49, 0.55, 0.67, 1.24, 1.60, and 2.26 μm
Algorithm derived surface reflectance at 0.412, 0.47, and 0.65 μm	Algorithm derived surface reflectance at 0.488, 0.67, and 2.25 μm
GEOS speciated AOD fractions	GEOS speciated AOD fractions
Cosine of Solar Zenith Angle, Scattering Angle, and Glint Angle	Cosine of Solar Zenith Angle, Scattering Angle, and Glint Angle

Table 1. Input features for the MODIS and VIIRS NNR algorithms over dark land surfaces (DT-Land and AERDT-Land, respectively)

MODIS	VIIRS
TOA reflectance at 412, 440, 470, 550, 660, 870, 1200, 1600, and 2100 nm	TOA Reflectance at 490, 550, 670, 860, 1240, 1610, and 2250 nm
GEOS speciated AOD fractions	GEOS speciated AOD fractions
Cosine of Solar Zenith Angle, Scattering Angle, and Glint Angle	Cosine of Solar Zenith Angle, Scattering Angle, and Glint Angle

Table 2. Input features for the MODIS and VIIRS NNR algorithms over ocean (DT-Ocean and AERDT-Ocean, respectively)

MODIS	VIIRS
TOA reflectance at 412, 440, 470, 550, 660, 870, 1200, 1600, and 2100 nm	TOA Reflectance at 412, 490, 550, 670, 1240, and 1610 nm
Algorithm derived surface reflectance at 412, 470, and 660 nm	Algorithm derived surface reflectance at 412, 480, and 670 nm
GEOS speciated AOD fractions	GEOS speciated AOD fractions

https://doi.org/10.5194/egusphere-2026-5508
Preprint. Discussion started: 29 September 2026

Cosine of Solar Zenith Angle, Scattering Angle, and Glint Angle	Cosine of Solar Zenith Angle, Scattering Angle, and Glint Angle

Table 3. Input features for the MODIS and VIIRS NNR algorithms over bright land surfaces (DB-deep and AERDB-deep, respectively)

Figure 1 shows the model performance for the three NNR models on the test dataset used during model development, which includes outlier points (see Figure S1 in the Supplementary Documentation for results excluding outliers). Overall, the NNR AOD estimates reduce the mean bias and root mean square error with respect to AERONET and significantly increase the correlation. When evaluated with the independent validation dataset (Figure 2), the evaluation statistics remain comparable, demonstrating generalizability of the model.

https://doi.org/10.5194/egusphere-2026-5508
Preprint. Discussion started: 29 September 2026

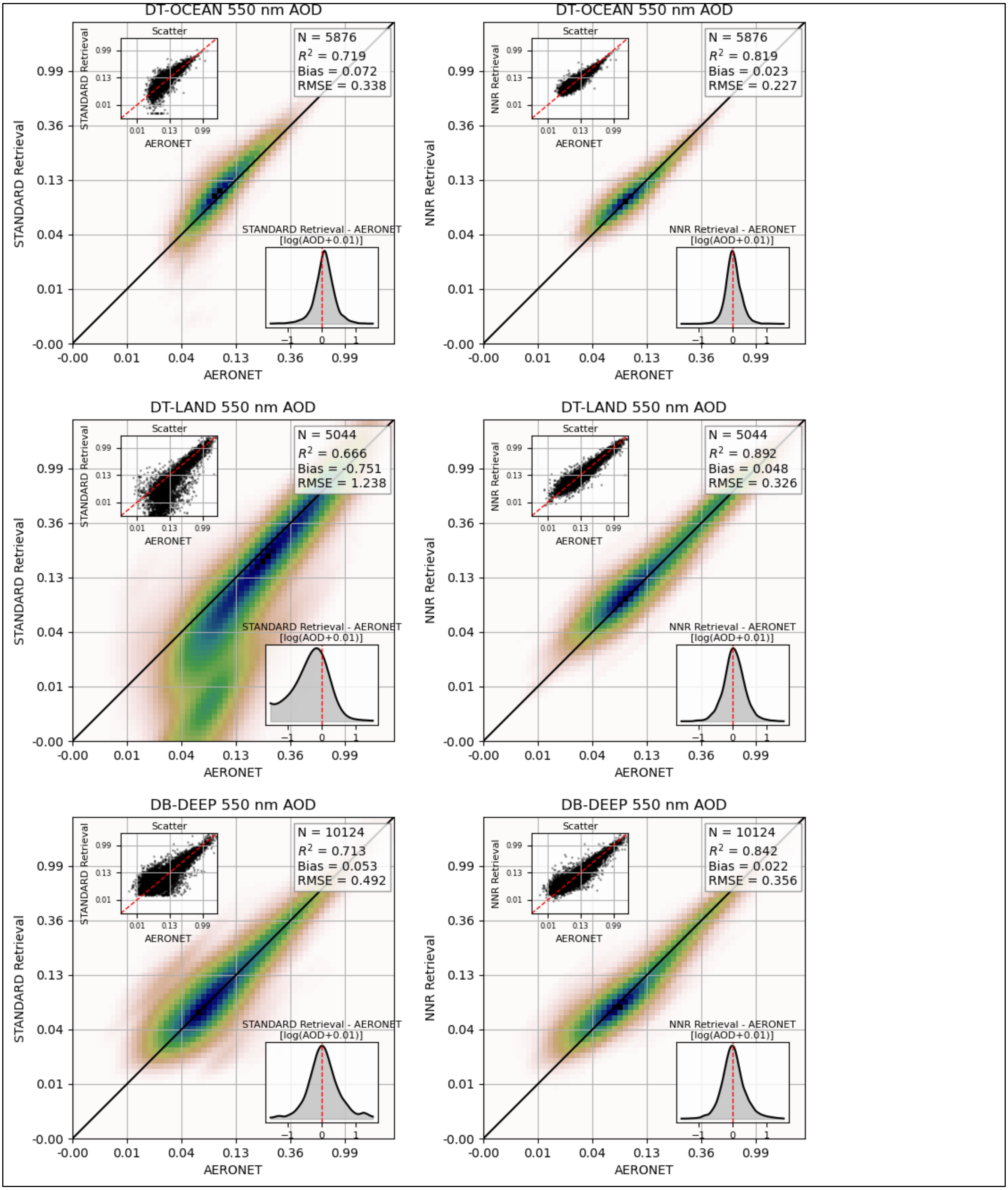

https://doi.org/10.5194/egusphere-2026-5508
Preprint. Discussion started: 29 September 2026

Figure 1: Comparison between satellite-AERONET colocations test dataset covering the time period of 2019-2024 used during model development for the three VIIRS retrieval algorithms. Figures on the left compare the standard AERDT and AERDB AOD products to AERONET, and figures on the right compare the NNR AOD predictions to AERONET.

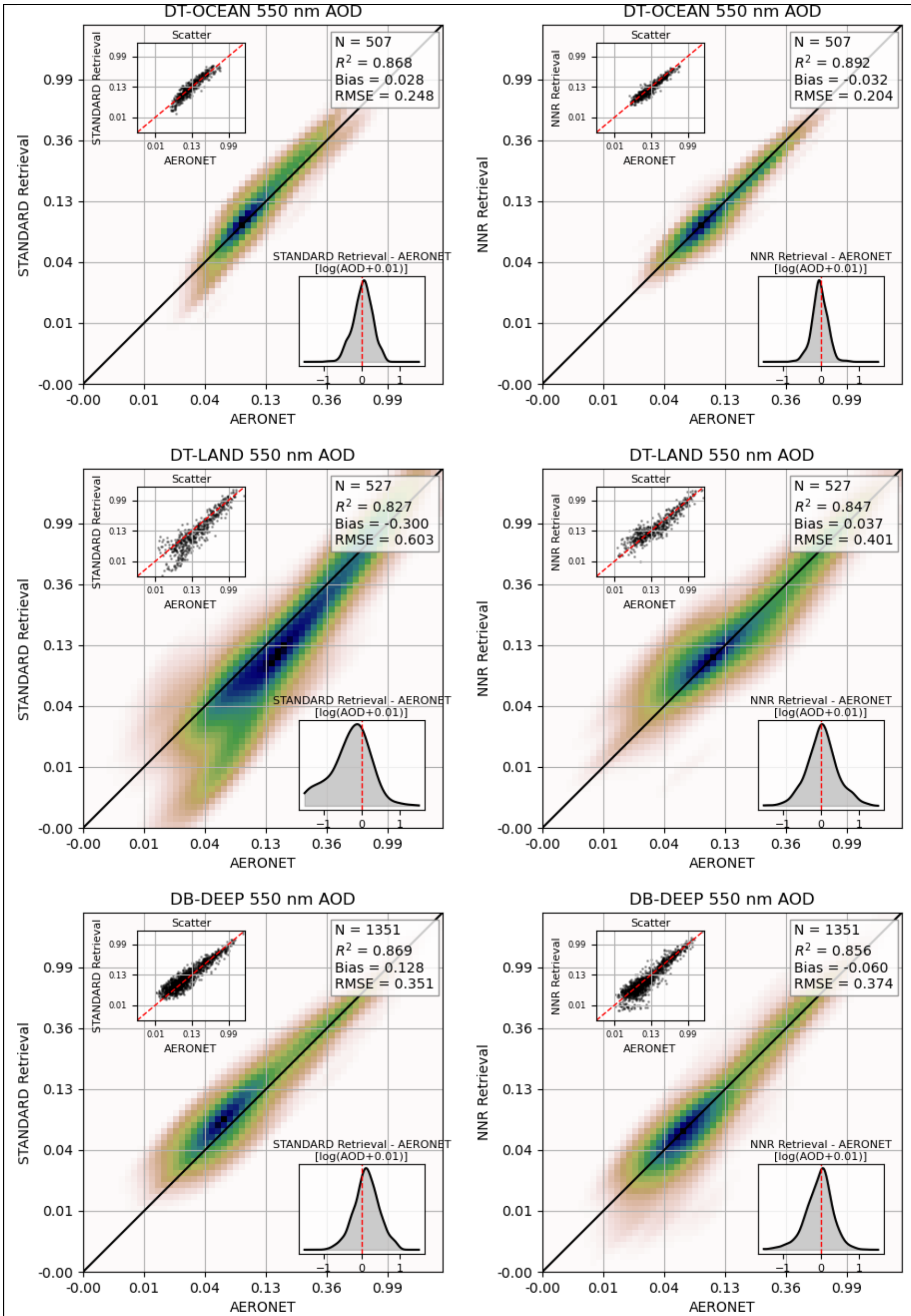

https://doi.org/10.5194/egusphere-2026-5508
Preprint. Discussion started: 29 September 2026

Figure 2: Comparison between satellite-AERONET colocations validation dataset for the year 2025. These are independent data, they were not used during model development for the three VIIRS retrieval algorithms. Figures on the left compare the standard AERDT and AERDB AOD products to AERONET, and figures on the right compare the NNR AOD predictions to AERONET.

Figure 3 shows seasonal means of MODIS and VIIRS NNR AOD predictions for the year 2019. Over oceans and dark land surfaces, the two products show generally good agreement, as expected given the similar overpass time of both sensors they are observing broadly similar aerosol conditions. Larger discrepancies emerge over bright surfaces, particularly across North Africa and other desert regions, where AOD retrieval are more sensitive to assumptions about surface reflectance. One likely contributor is that the MODIS and VIIRS Deep Blue algorithms rely on satellite-specific climatologies of surface reflectance, which may introduce systematic differences that alias into the retrieved AOD fields. Improved consistency may require adopting common surface reflectance characterization across retrieval instruments. Differences over high-latitude fire regions (e.g. Siberia and Canada) is less certain and require further validation, as the MODIS and VIIRS Dark Target algorithms apply different pixel selection criteria. Limited independent observations in these regions make attribution more difficult.

https://doi.org/10.5194/egusphere-2026-5508
Preprint. Discussion started: 29 September 2026

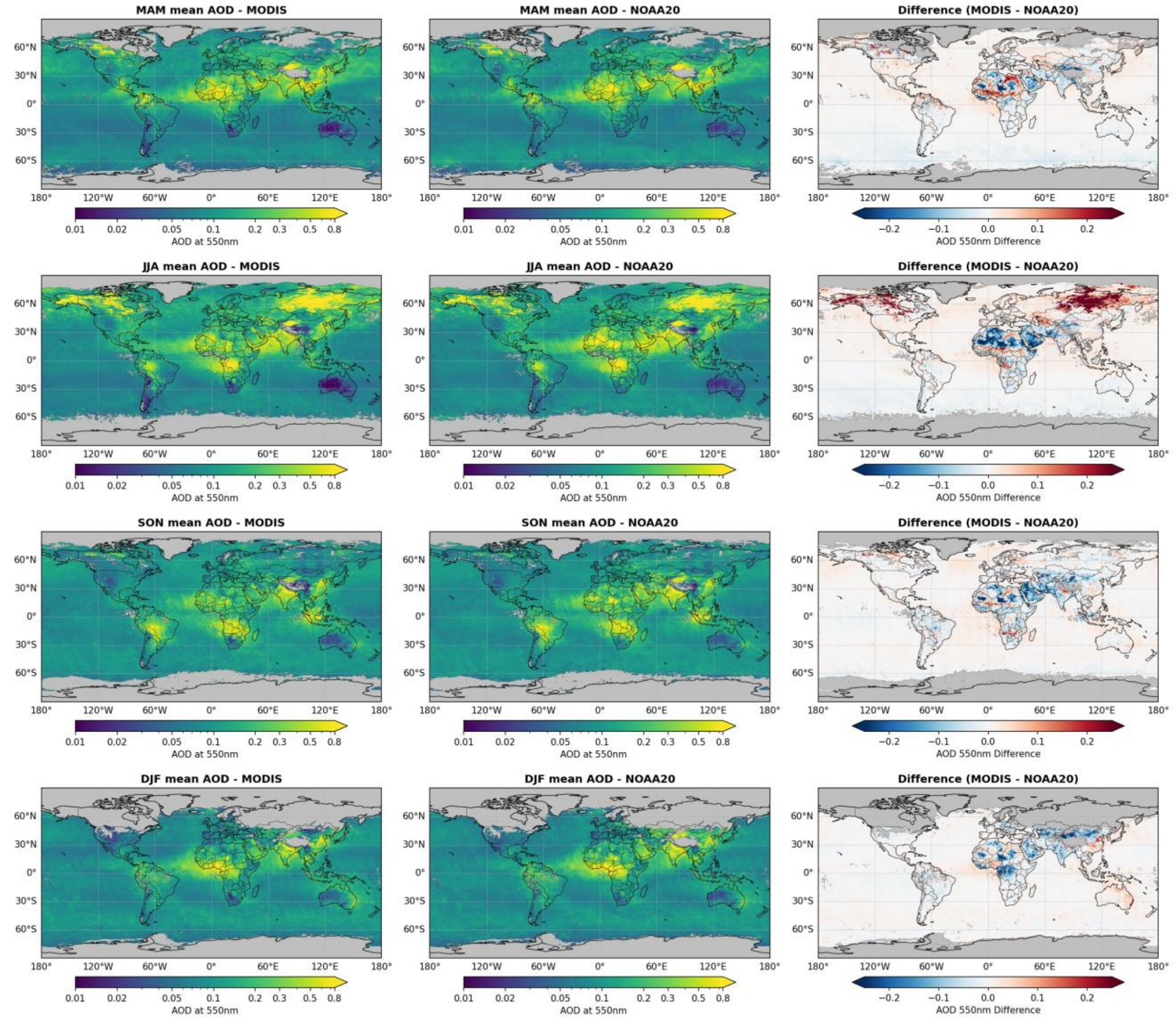

Figure 3. 2019 seasonal means of NNR AOD predictions for MODIS and VIIRS gridded to 0.25° x 0.3125° resolution.

Figure 4 shows the monthly mean MODIS and VIIRS NNR AOD from 2019-2025 for selected regions. Overall, the two datasets exhibit strong agreement in both seasonal and interannual variability and magnitude across most regions, indicating consistent large-scale aerosol estimates between the sensors (See Figure S2 for a comparison of the MODIS and VIIRS standard retrievals). The agreement is generally strongest over oceans and vegetated regions. Notably, the two regions dominated by bright surfaces (Australia and North Africa) show the largest differences between the two datasets. Some episodic discrepancies are also evident over North America during months with intense fire events. These extreme events are

https://doi.org/10.5194/egusphere-2026-5508
Preprint. Discussion started: 29 September 2026

likely under sampled in the VIIRS training dataset (which was trained on fewer years of AERONET collocations than MODIS) and may require future tuning to achieve better consistency between MODIS and VIIRS. In some regions, such as East Asia and South America, the difference between MODIS and VIIRS AOD estimates appear to be increasing over time. This would be consistent with the orbital drift occurring for the Aqua satellite, which began in 2021. This progressively altered the local observation time and results in the two sensors sampling different atmospheric scenes.

https://doi.org/10.5194/egusphere-2026-5508
Preprint. Discussion started: 29 September 2026

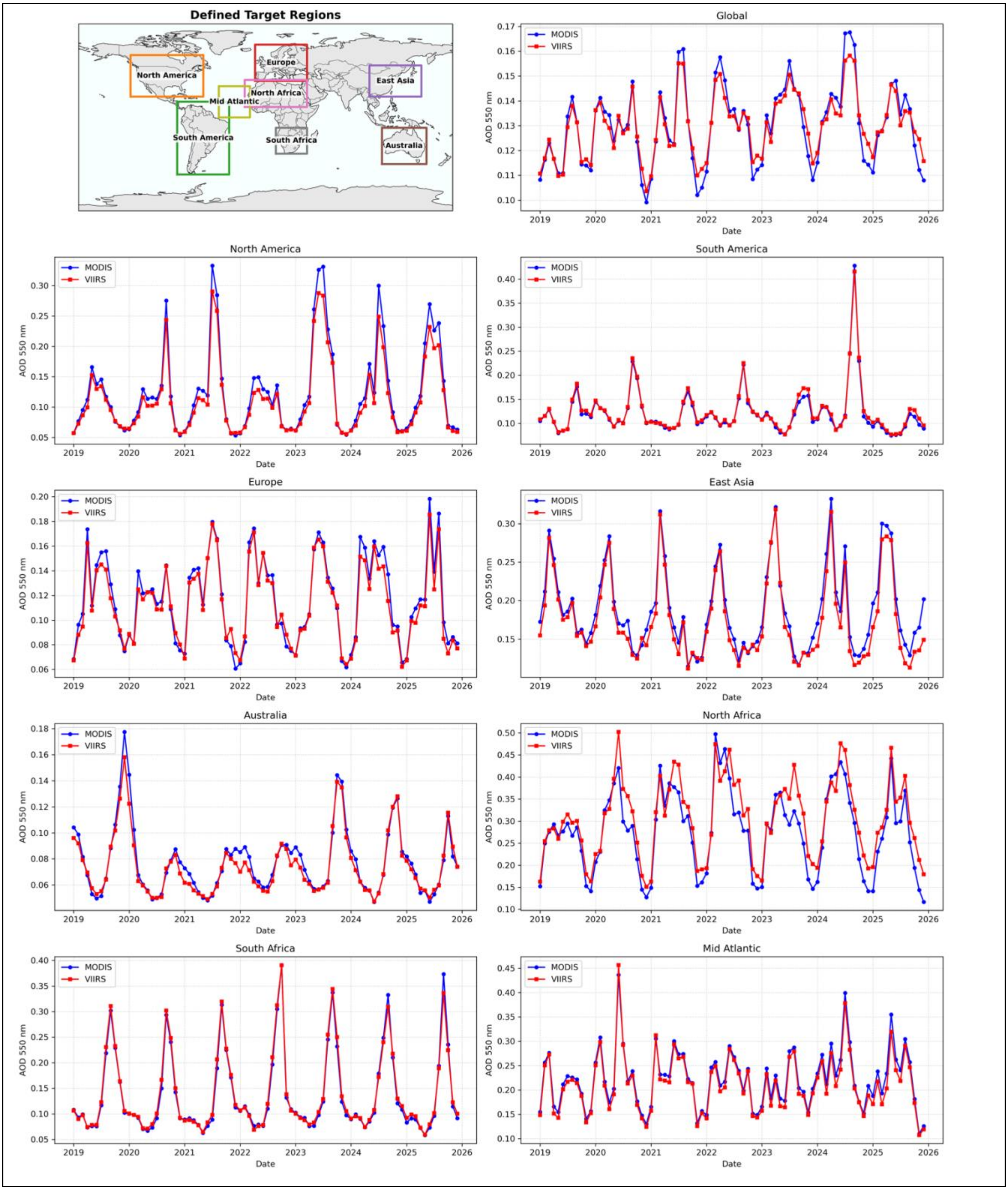

https://doi.org/10.5194/egusphere-2026-5508
Preprint. Discussion started: 29 September 2026

Figure 4. Monthly mean MODIS and VIIRS NNR AOD at 550 nm from 2019-2025 over selected global regions.

2.3 Data Assimilation Experiments

For computational efficiency, we performed the data assimilation experiments in replay mode which uses analyzed meteorological fields from the GEOS-IT reanalysis to constrain the models dynamical fields to follow the reanalysis rather than running the full meteorological data assimilation. This system utilizes a more recent version of the GEOS atmospheric model, but the same data assimilation system compared to the MERRA-2 configuration described by Gelaro et al. (2017). The model employs the same fundamental architecture with the GEOS atmospheric model coupled to the variational data analysis (3DVAR) Gridpoint Statistical Interpolation (GSI) meteorological analysis scheme. The discretization of the dynamical core is computed on a cubed sphere grid that mitigates grid-spacing singularities (Putman and Lin 2007).

For these experiments, the c180 model resolution on the native cubed-sphere grid corresponds to approximately 50 km horizontally, having 72 hybrid-eta vertical layers extending from the surface to 0.01 hPa. The GSI analysis system for the meteorology maintains the incremental analysis update procedure every 6 hours (Bloom et al. 1996), ensuring consistent meteorological constraint throughout the experimental period.

Two parallel experiments were conducted to evaluate the impact of different satellite AOD observations on aerosol analysis performance. Both experiments span from January 2019 through February 2020. The first two months serve as a model spin-up period, with our evaluation beginning from March 1, 2019, providing complete seasonal coverage through February 2020. The year 2019 was selected because it represents the final year in which both Terra and Aqua maintained their nominal orbits, providing maximum temporal overlap with VIIRS observations. After 2019, both satellites entered free-drift. Terra and Aqua executed their final inclination maneuvers in 2020 and 2021, respectively. Both satellites began to drift from their nominal equatorial crossing times, with Terra drifting earlier and Aqua later in local time. These orbital changes will introduce additional differences in observing conditions between the satellites, making interpretation of performance differences in the aerosol DA system more complex. Therefore, we restrict our analysis to a period prior to the MODIS orbital drifts.

Both experiments use identical versions of the GEOS model, emissions datasets, and meteorological fields; only the assimilated aerosol observations differ between the two experiments. To assimilate these NNR AOD observations, both experiments utilize the analysis splitting approach detailed in Section 2.1.2. Specifically, the aerosol assimilation is performed every 3 hours using the 2D Physical-Space Statistical Analysis System (PSAS) to compute the total AOD analysis increments, followed by the Local Displacement Ensemble (LDE) methodology, which translates these 2D increments into 3D mass concentration updates to vertically distribute the aerosol species.

https://doi.org/10.5194/egusphere-2026-5508
Preprint. Discussion started: 29 September 2026

2.3.1 Control experiment: MODIS Terra + Aqua assimilation

This experiment represents what is currently available in our operational system. It assimilates the NNR AOD products at 550 nm derived from the MODIS sensors aboard both the Aqua and Terra satellites, providing distinct morning and afternoon observational constraints. This run serves as our control experiment.

2.3.2 Test experiment: VIIRS NOAA-20 assimilation

This experiment evaluates the successor observing capability by assimilating the newly adapted VIIRS NNR AOD at 550 nm products from the NOAA-20 satellite. It follows the exact same harmonization methodology as the control but relies on the single NOAA-20 satellite platform rather than a dual-satellite constellation.

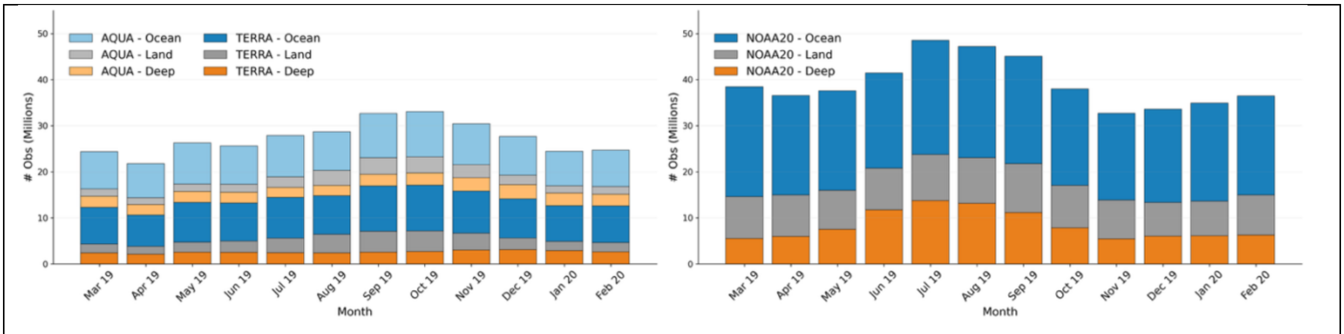

Figure 5: Left: Total global number of observations for 2019-early 2020 from MODIS Terra over ocean (dark blue), land (dark grey) and deep over bright surfaces (orange), from MODIS Aqua over ocean (light blue), land (light grey) and deep over bright surfaces (yellow). Right: Same for VIIRS NOAA-20 over ocean (dark blue), land (dark grey) and deep over bright surfaces (orange).

Figure 5 illustrates the temporal distribution and number of AOD observations available from MODIS (i.e. MODIS-control) and VIIRS NOAA-20 (i.e. VIIRS experiment) throughout the experimental period, highlighting the different observational coverage patterns between the two sensor systems. Notably, the VIIRS experiment provides more total observations than the MODIS-control experiment, even after combining both Terra and Aqua MODIS data.

Figure 6 illustrates the spatial and temporal coverage of observations assimilated in the MODIS-control versus the VIIRS experiment. A key difference emerges in the timing of observational constraints. The MODIS-control benefits from Terra's morning overpass (10:30 local solar time), providing observations over Africa during the 09Z assimilation cycle (shown in orange). As a result, the model is already constrained in the morning before the afternoon Aqua data arrives. Without this early coverage, the VIIRS experiment relies solely on the afternoon NOAA-20 observations, receiving its first African constraint during the 12Z cycle (13:30 local solar time). However, VIIRS offers compensating advantages: the sensor provides a wider swath width and significantly higher observation density (as shown in Figure 5) with potentially more clear-sky observing opportunities, though all observations occur simultaneously rather than being distributed across two overpass times. This trade-off fundamentally alters the temporal sampling. The dual-satellite MODIS constellation provides distinct morning and

https://doi.org/10.5194/egusphere-2026-5508
Preprint. Discussion started: 29 September 2026

afternoon observations. In contrast, the single NOAA-20 instrument provides primarily an afternoon constraint. However, the significantly wider VIIRS swath (~3040 km) ensures gapless daily coverage at the equator. Furthermore, at mid-to-high latitudes, the wide VIIRS swath results in consecutive overlapping orbits, providing multiple observations spanning from late morning through the afternoon that partially mitigate the loss of the morning satellite.

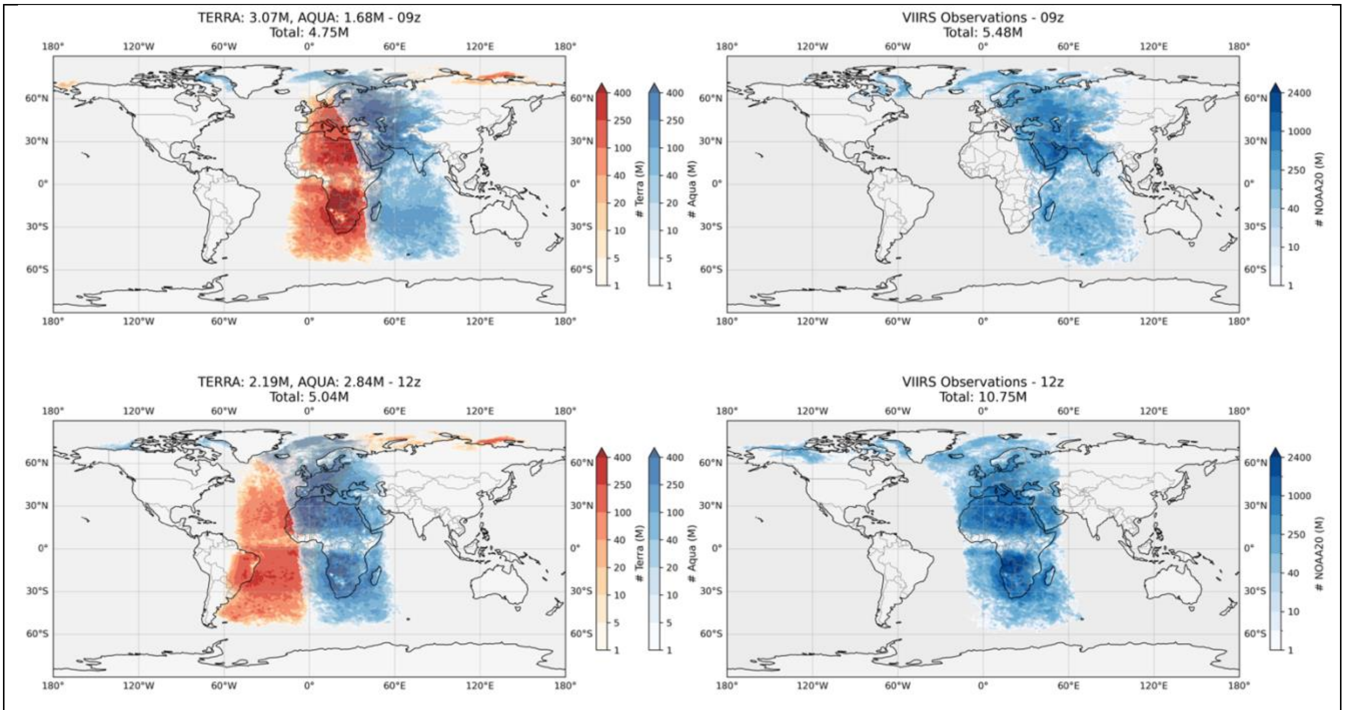

Figure 6: Synoptic time monthly mean number of observations for June 2019. Left: MODIS Terra (all retrieval algorithms including Dark Target and Deep Blue, in orange) and MODIS Aqua (all retrieval algorithms, in blue) for 09Z (top) and 12Z (bottom). Right: Same for VIIRS NOAA-20.

2.4 Evaluation Methods

2.4.1 Independent observations: AERONET and MAN datasets

As detailed in Section 2.2.1.1, AERONET provides high-accuracy, ground-based AOD measurements globally. While AERONET observations are used to train the NNR algorithm, the direct AERONET AOD measurements are not assimilated in either the MODIS-control or VIIRS experiments. Therefore, we utilize the quality-assured, cloud-screened Version 3 Level 2.0 AOD data (Giles et al., 2019) as an independent benchmark to validate the analyzed AOD fields. To assess model performance across diverse aerosol regimes, the simulated AOD outputs are collocated in space and time with AERONET observations during the study period.

https://doi.org/10.5194/egusphere-2026-5508
Preprint. Discussion started: 29 September 2026

For over-ocean validation, we utilize the Maritime Aerosol Network (MAN) (Smirnov et al., 2009). Operating as a ship-based component of AERONET, MAN provides valuable oceanic AOD measurements using handheld sun photometers, calibrated to achieve an estimated uncertainty of ±0.02. Like the land-based AERONET stations, MAN observations remain completely independent of our assimilation system, providing crucial validation for the analyzed AOD fields over marine environments.

2.4.2 Statistical metrics (bias, RMSE, correlation)

As stated previously, AOD is log-normally distributed due to the multiplicative nature of aerosol processes (Limpert et al., 2001). Therefore, the statistics presented in Section 3 are calculated as follows: X = ln(AOD + 0.01) where the offset of 0.01 prevents undefined values when AOD approaches zero. We then compute two key metrics:

$$\text{Mean Bias}=\overline{X_{model} - X_{obs}} \quad \text{Eq. 1}$$

$$RMSE = \sqrt{\overline{(X_{model} - X_{obs})^2}} \quad \text{Eq. 2}$$

Subtracting values in logarithmic space is mathematically equivalent to calculating their ratio, meaning these metrics evaluate relative rather than absolute differences. Consequently, the mean bias represents the systematic multiplicative bias, while the RMSE represents the typical multiplicative spread of the errors. By calculating these metrics in log-space, the multiplicative error factors remain consistent and robust across the full range of AOD values, from clean background conditions to high-loading extreme events.

3. Results

Our analysis begins by evaluating the AOD at 550 nm in both experiments, as this represents the primary aerosol parameter directly constrained by the assimilation process within GAAS. Other aerosol characteristics, including the speciation of aerosols, their vertical distribution, and the relationship between aerosol mass tracers and aerosol optical properties (e.g. individual aerosol species extinction, hygroscopic growth, absorption, and asymmetry parameters) remain indirectly influenced by the AOD assimilation. Rather, they are primarily governed by the underlying GEOS model physics, parameterization schemes, and the LDE methodology (Section 2.1.2), which redistributes the AOD analysis increments across aerosol species and vertical levels.

https://doi.org/10.5194/egusphere-2026-5508
Preprint. Discussion started: 29 September 2026

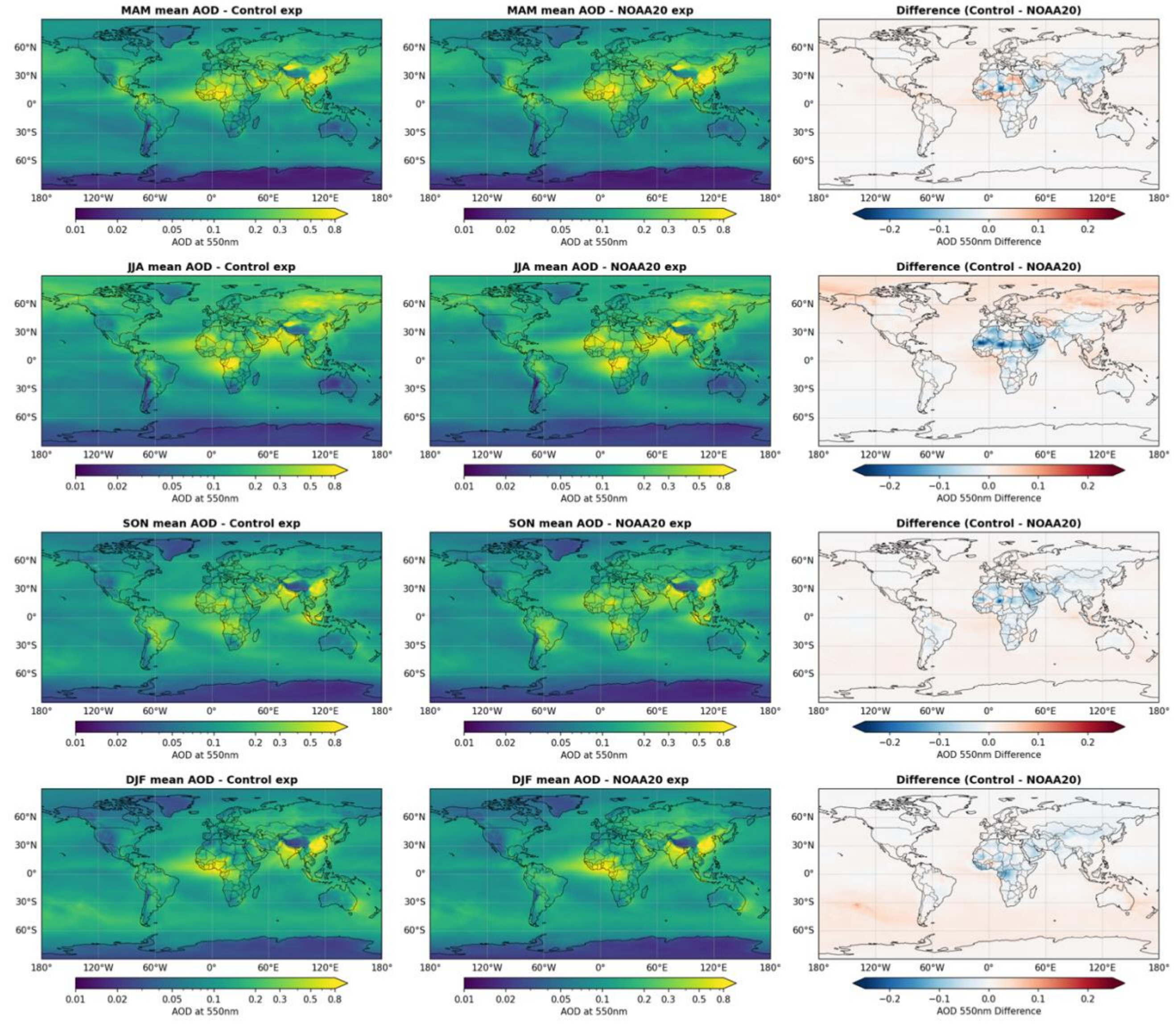

Figure 7: Seasonal-mean AOD at 550 nm for the Control experiment (left), NOAA-20 experiment (center), and their differences (Control minus NOAA-20, right) for March-April-May (MAM) 2019, June-July-August (JJA) 2019, September-October-November (SON) 2019, and December 2019-January-February 2020 (DJF).

Figure 7 shows comparisons of seasonal averaged predicted AOD at 550 nm for both experiments. In general, the MODIS-control and VIIRS experiments show comparable AOD patterns across most regions. However, several notable seasonal and regional differences emerge from the analysis.

Like Figure 3, over land, the two experiments exhibit similar AOD magnitudes except over bright desert surfaces, where differences become more pronounced during the primary dust season in summer (JJA). Note that Figure 3 represents co-located

https://doi.org/10.5194/egusphere-2026-5508
Preprint. Discussion started: 29 September 2026

comparisons between MODIS and VIIRS (only when both sensors are observing), while Figure 7 represents continuous seasonal averages even for times when observations are not available, and thus average differences appear smaller. During the JJA period, the VIIRS experiment consistently shows higher dust AOD compared to the MODIS-control, particularly across Northern African and Middle Eastern desert regions. Conversely, during the same JJA season, the VIIRS experiment displays systematically lower AOD values over the boreal regions of Siberia, Alaska, and northern Canada—areas characterized by intense wildfire activity during the summer months of 2019.

Additional differences occur in biomass burning regions during winter (DJF), where the VIIRS experiment response varies regionally. East of Australia, where intense wildfires produced significant biomass burning aerosol plumes, the VIIRS experiment exhibits lower AOD values compared to the MODIS Control. However, the pattern is not uniform across all fire-affected regions. The opposite pattern emerges over Central and West Africa during the DJF season—areas also affected by biomass burning during this period—where the VIIRS experiment shows higher AOD compared to the MODIS Control, indicating that the VIIRS experiment response to biomass burning observations varies regionally. These regional differences may be partly attributed to temporal sampling differences between the two systems: while MODIS provides two daily overpasses (Terra morning and Aqua afternoon), VIIRS provides primarily an afternoon constraint, potentially missing the early morning diurnal variability in biomass burning emissions and transport patterns.

The MAM season reveals another distinct pattern over Northern Africa, where the VIIRS experiment shows lower AOD in some regions while exhibiting higher values in adjacent areas, indicating spatially heterogeneous responses to the different satellite constraints during the spring dust season.

Over oceanic regions, the differences between the two experiments are generally subtle across all seasons, with the VIIRS experiment showing a slight but systematic tendency to produce lower sea salt aerosol loading compared to the MODIS-control.

A closer look at these differences is provided in Section 3.2 through comparisons with independent observations from the AERONET and MAN networks, which offers ground-based validation datasets not used in either assimilation system.

https://doi.org/10.5194/egusphere-2026-5508
Preprint. Discussion started: 29 September 2026

3.1 Analysis Performance

3.1.1 AOD innovation statistics

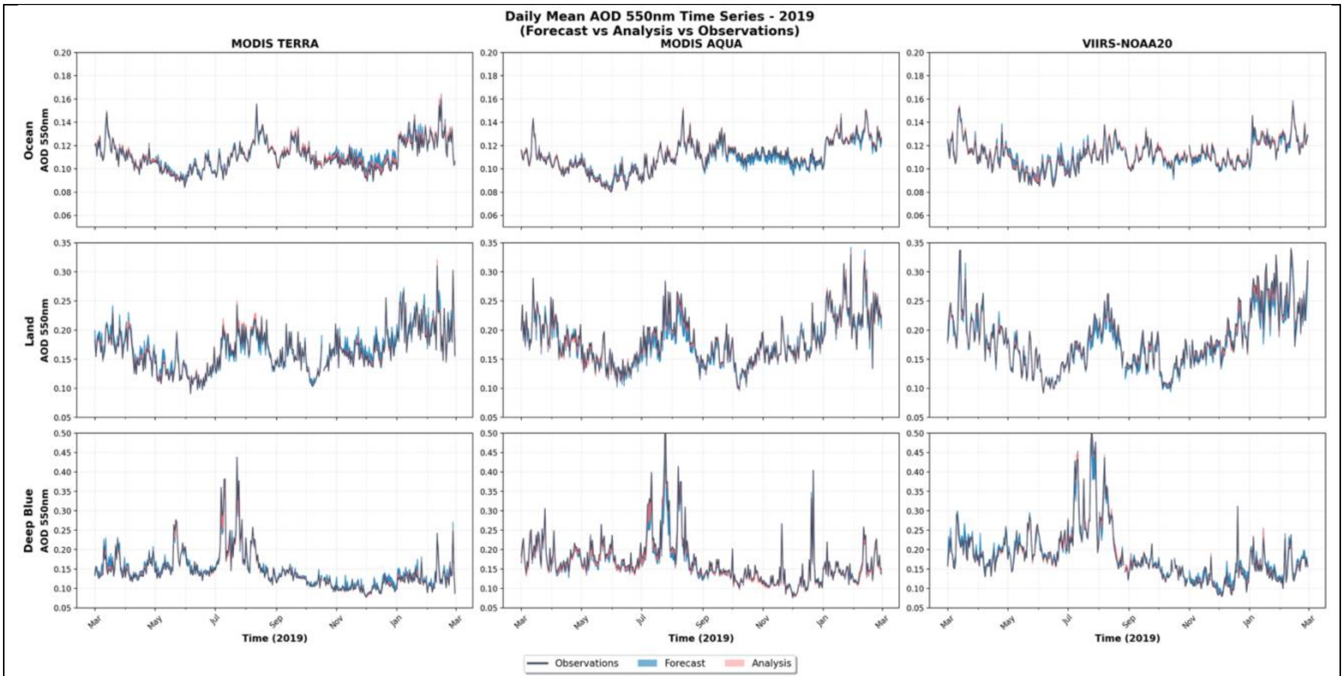

Figure 8: Collocated daily time series of observed (black) and model forecasted (blue) AOD at 550 nm from MODIS Terra NNR, MODIS Aqua NNR, and VIIRS NOAA-20 NNR, displayed separately for ocean, land, and deep blue retrievals. Analysed (assimilated) states are shown in red. Note the different y-axis scales used to capture high AOD events over land and deep blue retrievals.

Figure 8 shows collocated daily global mean time series of observed (O, in black) and model forecasted (F, in blue) AOD from MODIS Terra NNR, MODIS Aqua NNR, and VIIRS NOAA-20 NNR, displayed separately for Dark Target Ocean, Land, and Deep Blue retrievals on different scales (y-axis) to capture high AOD events over land and deep blue. The analysis (A) values are also shown in red, representing the assimilated state that combines the forecast and observations. These comparisons serve as a visual validation of the data assimilation system's performance, as the analysis is expected to yield improved overall statistics with respect to the assimilated observations compared to the forecast alone.

The time series reveal several important characteristics of the assimilation system. First, the analysis is usually closer to the observations than the forecast for all three instruments, confirming that the assimilation process is functioning as expected. Comparing across instruments, VIIRS NOAA-20 shows similar temporal patterns to both MODIS instruments throughout 2019 into early 2020, indicating good consistency in capturing seasonal and episodic aerosol variations. The Deep Blue NNR retrievals show the largest variability and occasional high AOD episodes, likely capturing dust events and biomass burning

https://doi.org/10.5194/egusphere-2026-5508
Preprint. Discussion started: 29 September 2026

plumes that can be challenging for the model to predict without observational constraints (where F is lower than O). Outside of these peak events, the baseline forecast tends to overestimate AOD relative to both Terra and VIIRS (F > O). For Aqua, however, the forecast aligns much more closely with the observations, demonstrating the corrective impact of the earlier Terra assimilation within the Control experiment.

Ocean NNR retrievals exhibit a smooth temporal evolution and small observation-forecast departures, reflecting the generally low aerosol variability over marine regions. While VIIRS shows slightly larger departures than MODIS during spring and summer, it demonstrates superior stability during fall and winter (September–December) when the two MODIS instruments diverge—with Terra indicating forecast overestimation (F > O) and Aqua indicating underestimation (F < O). Regardless of these seasonal nuances, marine AOD is typically very low (<0.15), making these absolute differences minor and well within expected inter-instrument variations.

Land NNR retrievals exhibit moderate variability driven by dust, smoke, and pollution, with observation-forecast departures showing distinct seasonal and instrument-specific trends. In summer, the forecast underestimates AOD (F < O) across all instruments, including Aqua, despite the earlier assimilation of Terra data. During fall and winter, the Control experiment's morning forecast overestimates Terra (F > O) but aligns closely with Aqua in the afternoon, further highlighting the corrective impact of the earlier Terra assimilation. Conversely, the separate VIIRS experiment persistently underestimates AOD (F < O) throughout these months. Despite these varying baselines, the assimilation system consistently and effectively pulls the analysed state toward the observations.

3.1.2 Comparisons relative to independent observations

3.1.2.1 Over land: Global AERONET comparisons

We assess the performance of the analysed AOD fields at 550 nm by comparing them with independent AERONET observations, which are not assimilated in either experiment. These comparisons are performed for both the Control and VIIRS experiments to examine the overall impact of transitioning from MODIS to VIIRS AOD assimilation. AERONET provides valuable independent validation due to its high accuracy and global coverage. The validation is conducted through seasonal comparisons to capture the temporal variability in aerosol processes and assimilation performance from March 2019 through February 2020.

https://doi.org/10.5194/egusphere-2026-5508
Preprint. Discussion started: 29 September 2026

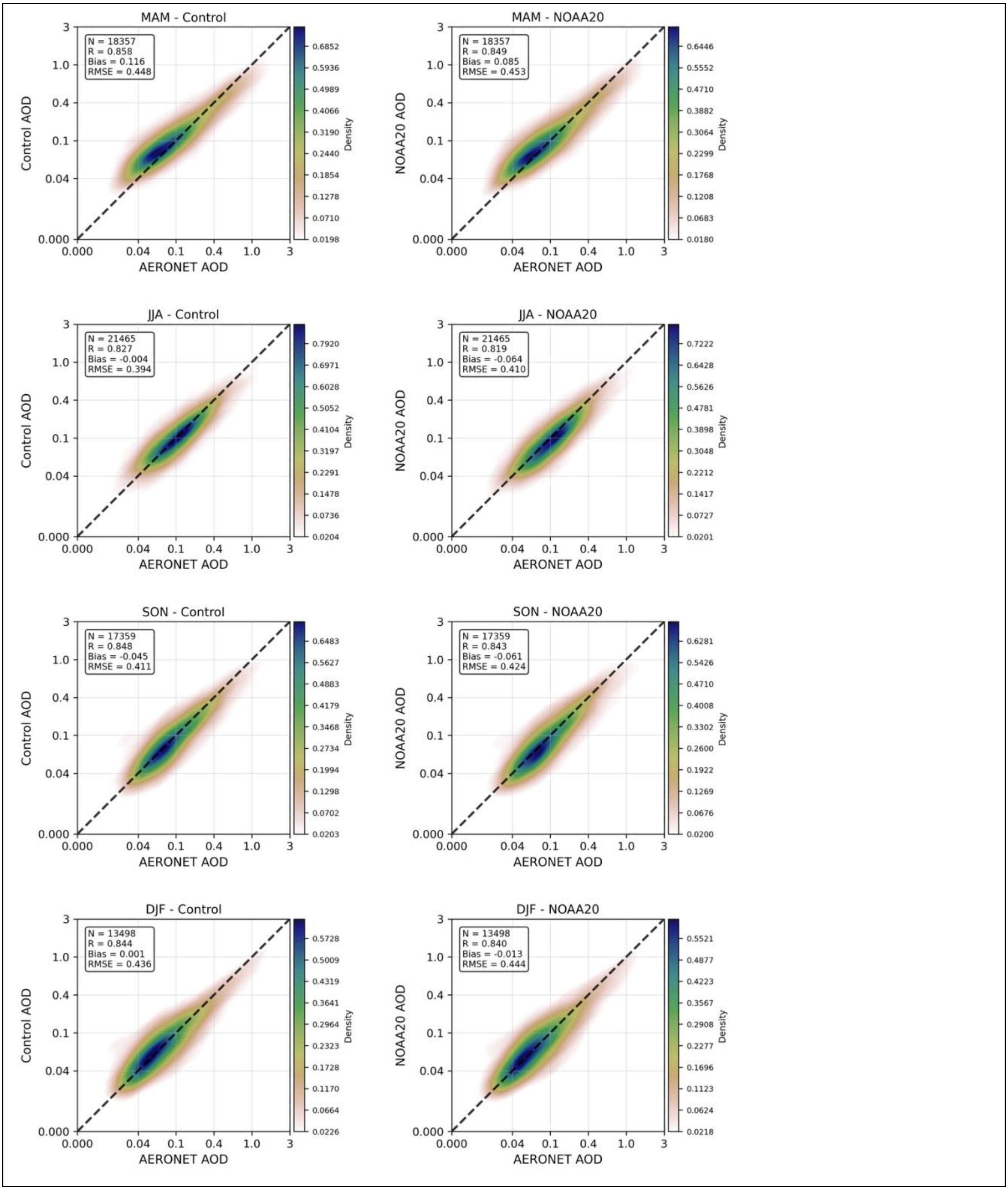

https://doi.org/10.5194/egusphere-2026-5508
Preprint. Discussion started: 29 September 2026

Figure 9: Seasonal density scatter plots comparing collocated simulated AOD against AERONET observations for the Control (left) and NOAA-20 (right) experiments across the four seasons of 2019–early 2020. Statistical metrics (N, R, Bias, RMSE) are computed in log-space and displayed for each season.

Figure 9 presents seasonal density scatter plots of the collocated daily mean analyzed AOD against AERONET observations for both experiments. The distributions reveal that the statistical performance is very similar globally between the two systems, with both achieving very good correlations with AERONET observations across all four seasons. With the validation strictly focused over land (including the bright surfaces), both the MODIS-control and VIIRS experiments demonstrate highly consistent, low biases and comparable RMSE values throughout the year. While the overall global performance is nearly identical, any remaining, marginal seasonal differences between the experiments likely reflect the varying influence of different aerosol source regions and transport patterns throughout the year (as seen in Figure 7), as well as instrument-specific retrieval characteristics under varying atmospheric conditions.

3.1.2.2 Regional Analysis

Figure 10 compares simulated AOD to observations from AERONET stations globally during March 2019 through February 2020. Statistics are computed in log space based on hourly observations and collocated model output from both the Control (MODIS) and NOAA-20 experiments. For most stations, both experiments demonstrate high correlations (0.6-0.9) with observed AOD, indicating that the assimilation system effectively captures aerosol variability across diverse environmental conditions and aerosol regimes.

The spatial distribution of performance statistics reveals that correlation coefficients are similar between experiments, with both maintaining strong agreement with AERONET observations worldwide. Biases and RMSE values show generally comparable magnitudes between experiments globally, with mixed spatial patterns where NOAA-20 shows lower errors (bias and RMSE) at some specific sites (e.g. Tamanrasset and Kanpur), and higher at some other sites, indicating no systematic global advantage for either system during the period of study. Notably, the similar correlation and RMSE patterns suggest that both MODIS and VIIRS observational constraints effectively guide the assimilation system toward realistic AOD temporal variability. Despite both datasets being bias-corrected against AERONET through the NNR algorithm, systematic bias differences persist in the assimilated fields, likely reflecting residual differences in instrument sampling characteristics, retrieval sensitivities under different atmospheric conditions, or temporal/spatial coverage patterns that affect the assimilation process, as well as GEOS model biases. Note that unlike Figure 1 & 2, the comparisons in Figure 10 also include AERONET observations that are not coincident with satellite overpass.

https://doi.org/10.5194/egusphere-2026-5508
Preprint. Discussion started: 29 September 2026

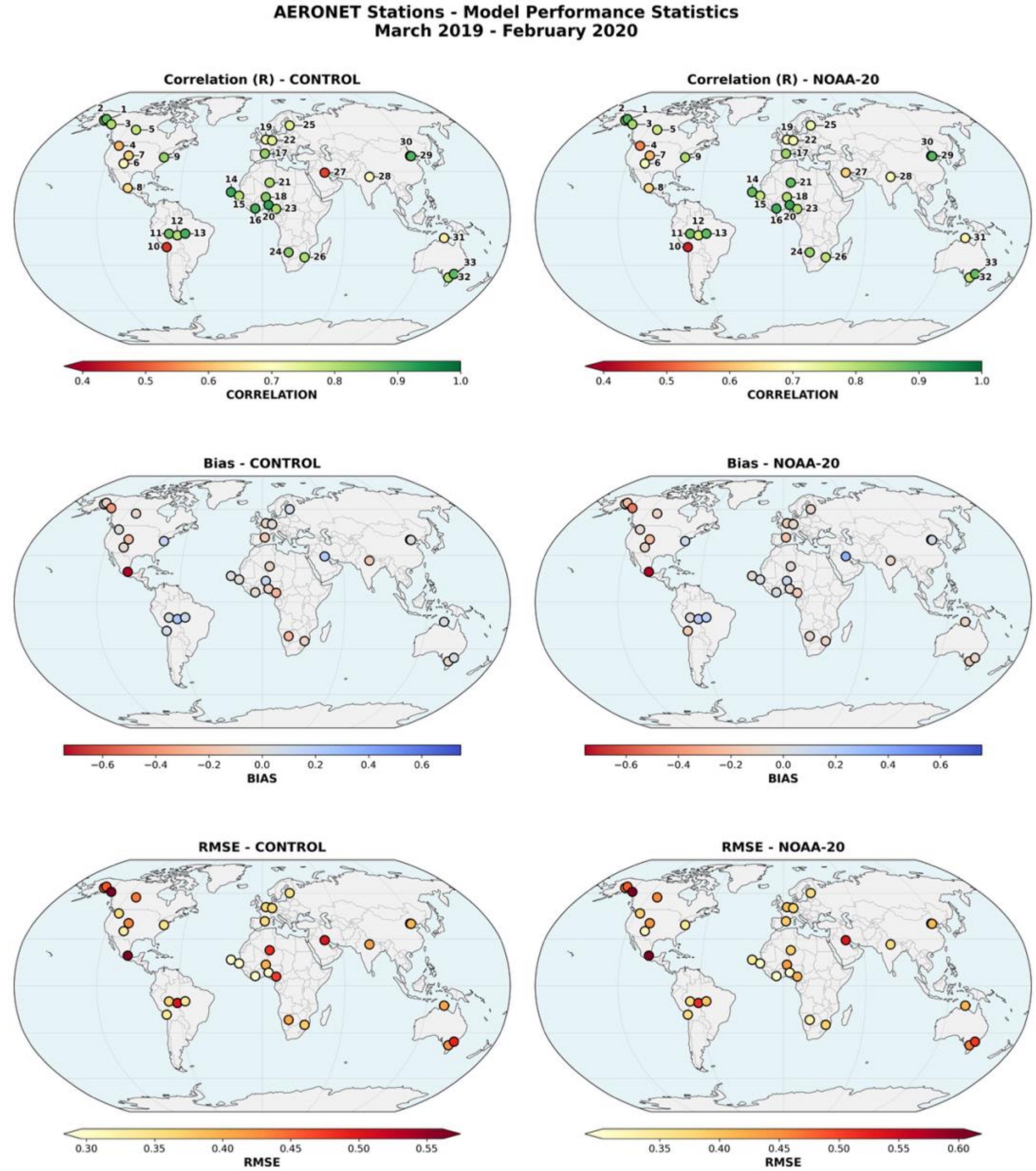

#	Station	Country	#	Station	Country	#	Station	Country	#	Station	Country
1	NEONHEAL	United States	10	Arica	Chile	19	Lille	France	28	Kanpur	India
2	BonanzaCreek	United States	11	RioBranco	Brazil	20	Ilorin	Nigeria	29	Beijing	China
3	KluaneLake	Canada	12	JiParanaSE	Brazil	21	Tamanrasset	Algeria	30	XiangHe	China
4	Rimrock,ID	United States	13	AltaFloresta	Brazil	22	Mainz	Germany	31	Jabiru	Australia
5	FortMcKay	Canada	14	CapoVerde	Sal Island	23	Bamenda	Cameroon	32	Aspendale	Australia
6	Sanda,NM	United States	15	Dakar	Senegal	24	Bonanza	Namibia	33	Tumbarumba	Australia
7	Boulder,CO	USA	16	CoteIvoire	Côte Ivoire	25	Helsinki	Finland			
8	MexicoCity	Mexico	17	Barcelona	Spain	26	Skukuza	South Africa			
9	GSFC,MD	USA	18	Banizoumbou	Niger	27	ShagayaPark	Kuwait			

Figure 10: Global spatial distribution of model performance statistics (Correlation, Bias, and RMSE) compared against AERONET observations during March 2019 through February 2020 for the Control experiment (left) and NOAA-20 experiment (right). Statistics are computed in log-space based on hourly collocations.

https://doi.org/10.5194/egusphere-2026-5508
Preprint. Discussion started: 29 September 2026

We then conducted detailed comparisons at key AERONET sites representing different aerosol regimes. These time-series comparisons provide insight into how the assimilation of VIIRS versus MODIS AOD handles specific aerosol types and extreme events.

Figure 11 presents the time series for key dust-dominated and mixed-aerosol sites across Northern and Western Africa (Tamanrasset (#21), Banizoumbou (#18), Dakar (#15), and Cabo Verde (#14)) during the summer months (JJA) of 2019. The region exhibits complex seasonal performance patterns, with distinct behavior emerging in pure dust versus coastal environments.

Tamanrasset (Algeria), located in the central Sahara, serves as an excellent pure dust validation site. Here, the VIIRS NOAA-20 experiment demonstrates strong performance, particularly in capturing higher dust loading events during the peak Saharan dust transport season. Throughout the summer, VIIRS consistently produces AOD values that align closely with AERONET observations, occasionally outperforming MODIS, which may be attributed to VIIRS's higher spatial resolution allowing for more spatially representative observations. Moving west to the Sahel and coastal regions, Banizoumbou (Niger) and Dakar (Senegal) show generally comparable results between the VIIRS and MODIS experiments, effectively capturing the summer dust variations. However, Banizoumbou shows slightly better agreement in the VIIRS experiment, which successfully picks up higher episodic dust events in June.

Conversely, Cabo Verde, an island site off the western coast of Africa influenced by both transported Saharan dust and marine aerosols, reveals a systematic underestimation with VIIRS data assimilation compared to MODIS. This coastal site captures the transition zone between continental dust sources and maritime transport, highlighting the tendency of VIIRS to retrieve lower AOD values in marine environments even when substantial dust loading is present. This behavior is consistent with the broader pattern of VIIRS slight underestimation over oceanic regions observed in the global statistics. More comprehensive comparisons will be conducted with the Maritime Aerosol Network (MAN) over open ocean regions in the next section.

https://doi.org/10.5194/egusphere-2026-5508
Preprint. Discussion started: 29 September 2026

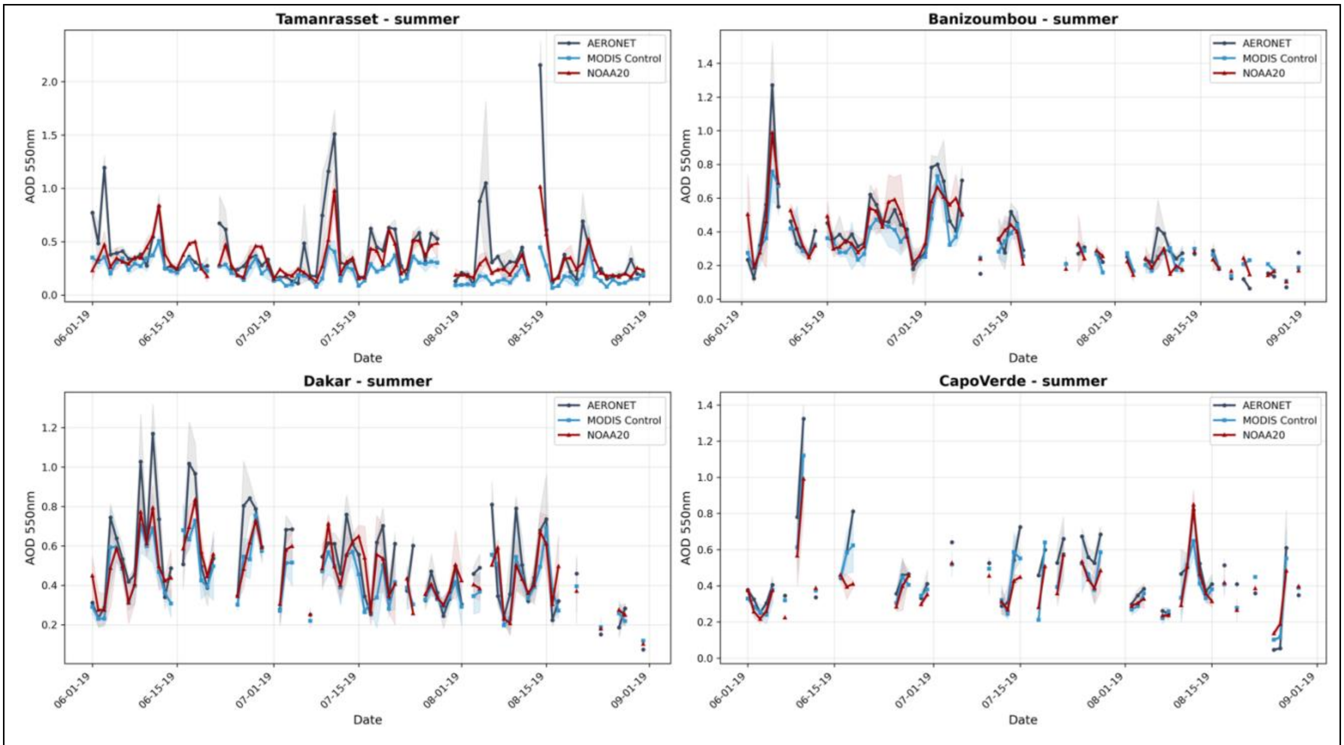

Figure 11: Time series of daily mean aerosol optical depth (AOD) at 550 nm from AERONET observations (black) alongside the Control (blue) and NOAA-20 (red) model experiments, which have been collocated in space and time at the observation locations. Data are shown for four key dust-dominated and coastal sites in Northern and Western Africa (Tamanrasset, Banizoumbou, Dakar, and Capo Verde) during summer (JJA) 2019.

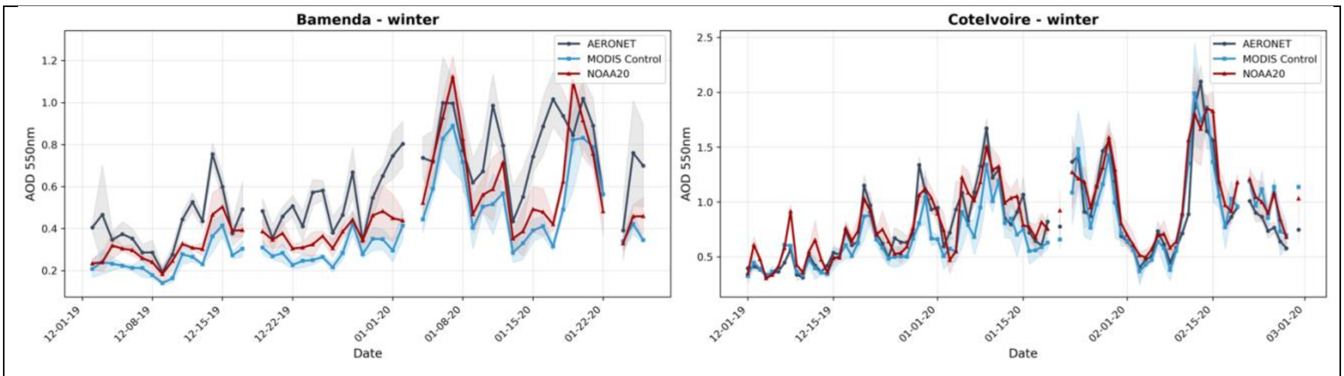

Figure 12: Same as Fig. 11 but for mixed-aerosol sites at Bamenda (Cameroon highlands) and Côte d'Ivoire during the winter months (DJF) 2019–2020.

Figure 12 illustrates the wintertime (December 2019–February 2020) time series for Bamenda (#23), located in the Cameroon highlands, and a coastal site in Côte d'Ivoire (#16). During this period, these regions experience a complex mixture of

https://doi.org/10.5194/egusphere-2026-5508
Preprint. Discussion started: 29 September 2026

transported Saharan dust and intense local biomass burning (Eck et al., 2010; Giglio et al., 2006). Overall, both assimilation experiments perform well in capturing the daily AOD variability, closely tracking the dynamic temporal evolution of the AERONET observations. However, their ability to capture peak aerosol magnitudes differs by location. At Bamenda, both experiments systematically underestimate the high AOD peaks. This persistent low bias is probably driven by the model experiments ~50 km horizontal resolution, which smooths the sharp highland topography and creates a mismatch between the model's average grid box elevation and the actual station elevation, thereby altering the assumed atmospheric column depth. At the Côte d'Ivoire site, the performance is more nuanced. Both the MODIS Control and NOAA-20 experiments perform remarkably similarly, remaining very close to each other throughout the season. Rather than one system showing a definitive advantage, they alternate in their agreement with AERONET. This alternating performance demonstrates that while the specific constraints from each sensor differ, both observing systems provide acceptable results in these challenging, highly variable mixed-aerosol environments.

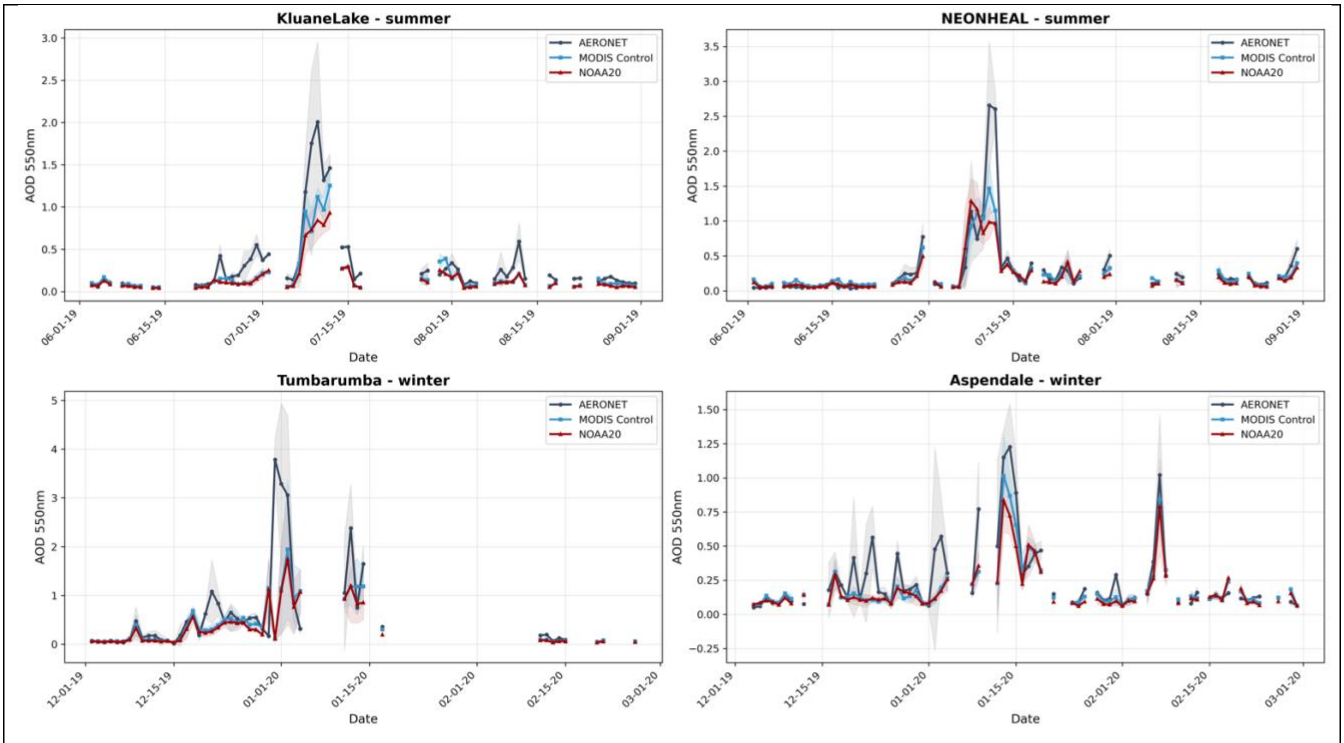

Figure 13: Same as Fig. 11 but for extreme biomass burning influenced sites during the boreal wildfires (Kluane Lake and NEONHEAL, JJA 2019) and the Australian bushfires (Tumbarumba and Aspendale, DJF 2019–2020).

The assimilation systems were further evaluated under extreme biomass burning conditions, specifically during the intense boreal wildfires of summer (JJA) 2019 and the unprecedented Australian bushfires during the winter (DJF) 2019–2020 season.

https://doi.org/10.5194/egusphere-2026-5508
Preprint. Discussion started: 29 September 2026

Figure 13 presents the time series for affected AERONET sites: Kluane Lake (Yukon, Canada, #3) and NEONHEAL (Alaska, USA (#1)) for the boreal fires, alongside Tumbarumba (#33) and Aspendale (#32) for the Australian fires. During these periods, AERONET recorded exceptionally high episodic AOD values, frequently exceeding 2.0 and occasionally reaching as high as 4.0 to 5.0. Both the MODIS Control and VIIRS NOAA-20 experiments demonstrate a strong ability to track the rapid temporal variability and timing of these extreme smoke plumes, performing very closely to one another throughout the seasons. However, both models systematically underestimate the absolute peak AOD magnitudes during the most intense fire events. This underestimation is a known challenge in global modelling of extreme wildfires, often resulting from a combination of rapid diurnal emission changes, complex plume injection heights, and the dilution of highly concentrated smoke plumes within the model's ~50 km grid boxes. While the performance of both experiments is highly comparable, the MODIS Control experiment exhibits a slight advantage over the NOAA-20 experiment, capturing slightly higher AOD peaks that bring it marginally closer to the AERONET observations. This subtle advantage is likely attributable to the temporal sampling differences between the satellite systems; the combined Terra (morning) and Aqua (afternoon) overpasses provide two daily observational constraints, which may better capture the rapid diurnal evolution and transport of intensive wildfire emissions compared to the afternoon overpass provided by VIIRS.

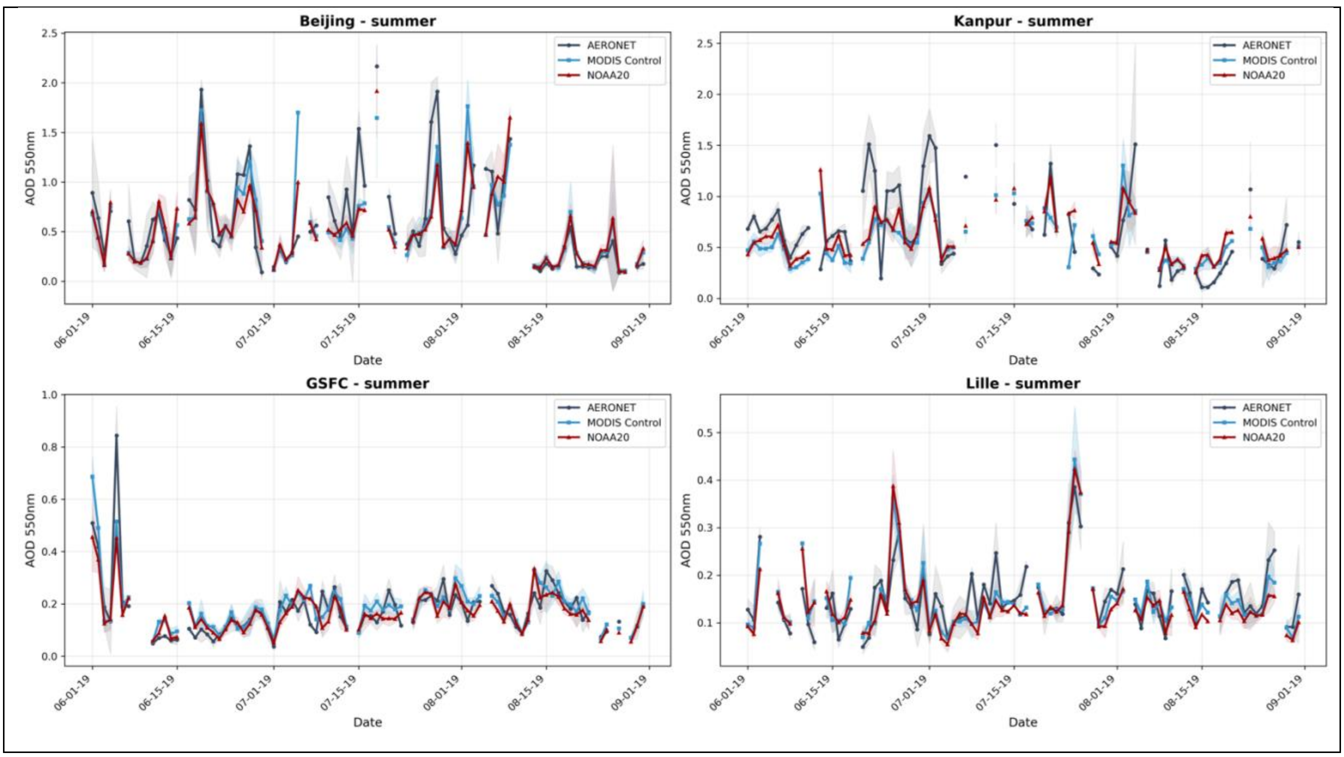

https://doi.org/10.5194/egusphere-2026-5508
Preprint. Discussion started: 29 September 2026

Figure 14: Same as Fig. 11 but for urban and industrial polluted regimes at Beijing (China), Kanpur (India), GSFC (United States), and Lille (France) during summer (JJA) 2019.

The final set of time-series comparisons (Figure 14) focuses on urban and industrial polluted regimes during the summer (JJA) of 2019, featuring AERONET sites at Beijing (China, #29), Kanpur (India, #28), GSFC (United States, #9), and Lille (France, #19). Among these locations, Beijing and Kanpur record the highest overall AOD values, reflecting heavy regional anthropogenic emissions and the complex mixture of industrial pollution with seasonal aerosols. In contrast, GSFC and Lille represent typical North American and European urban environments with more moderate AOD loadings. Across all four sites, the MODIS Control and VIIRS NOAA-20 experiments perform similarly. Both systems successfully track the daily AERONET AOD variability, and both tend to underestimate the magnitude of major peak pollution events. This nearly identical performance demonstrates continuity in the aerosol analysis when transitioning from MODIS to VIIRS over globally polluted regions.

3.1.2.3 Over Ocean: MAN comparisons

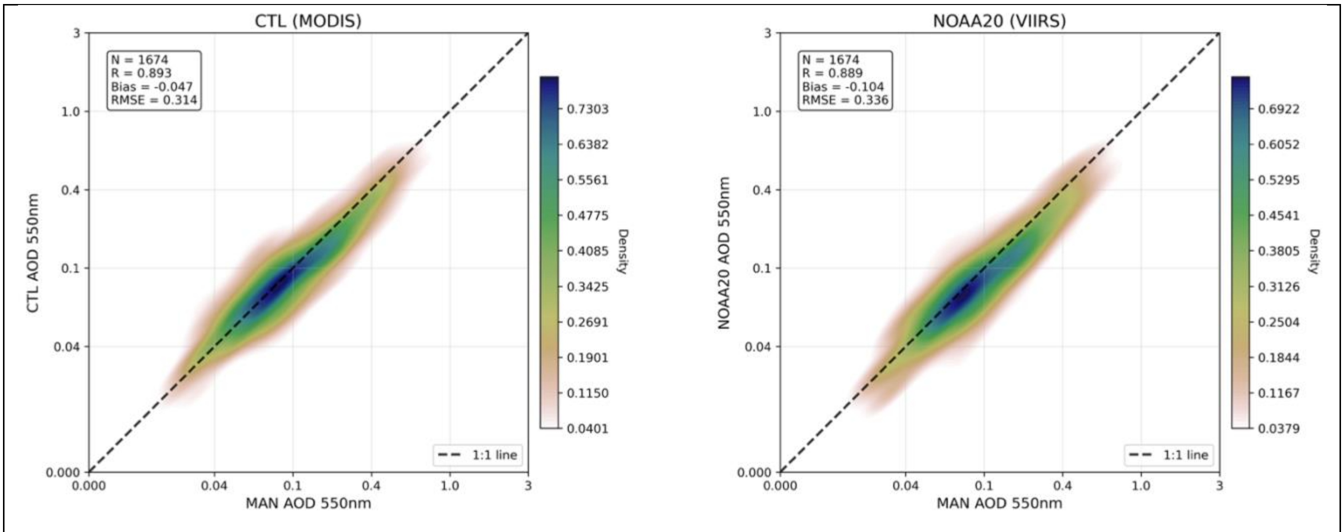

Figure 15: Density scatter plots comparing all available Maritime Aerosol Network (MAN) AOD observations at 550 nm with collocated modeled AOD from the Control experiment (left) and NOAA-20 experiment (right) during 2019 through early 2020. Statistical metrics (N, R, Bias, RMSE) are displayed for each experiment.

Figure 15 compares all available MAN observations with co-located modeled AOD from the MODIS control (left) and VIIRS experiment (right) during 2019 through early 2020. Both experiments show strong correlations with MAN observations and generally low biases. However, the NOAA-20 experiment tends to slightly underestimate MAN observations, which directly

https://doi.org/10.5194/egusphere-2026-5508
Preprint. Discussion started: 29 September 2026

reflects the systematic pattern of slightly reduced sea salt loading over oceanic regions compared to the MODIS Control (Figure 7). Despite this slight underestimation, given the typically low AOD values over the ocean (generally < 0.15), the VIIRS assimilation results remain highly acceptable; the overall bias sits well within the MAN uncertainty (± 0.02), and the system maintains a high correlation with the observations.

4. Discussion and Conclusions

The agreement between the independent observations and the analysis assimilating all three VIIRS NNR products (Ocean, Land, and Deep Blue) throughout 2019 and early 2020 provides confidence that VIIRS NOAA-20 NNR observations can be effectively assimilated within the NASA GEOS system. A feature of the GMAO aerosol assimilation framework is its reliance on the Neural Network Retrieval (NNR) methodology, which translates cloud-cleared top-of-atmosphere satellite radiances directly into AERONET-calibrated AOD. By developing an algorithm for the VIIRS sensor, the system effectively homogenizes the distinct observing platforms, mitigating instrument-specific biases related to varying instrument characteristics, observing geometries, and cloud cover criteria prior to assimilation. Global validation against independent AERONET and MAN observations demonstrates that the VIIRS NOAA-20 experiment maintains strong spatial correlations and comparable RMSE globally, proving highly capable of matching the performance of the dual-satellite MODIS constellation.

Detailed regional time-series analyses highlight the specific strengths and shared limitations of the constraints the observing systems and employed algorithms can provide across diverse aerosol regimes. In pure dust environments, particularly over the Sahara and Sahel, the VIIRS experiment frequently aligned closer to AERONET observations than the MODIS Control. This advantage is largely attributable to the higher spatial resolution and wider swath of VIIRS, which provides a higher density of valid observations, better spatial representation in complex, dusty environments. Over heavily polluted urban and industrial regions, the two systems demonstrated nearly identical performance, effectively capturing the daily temporal variability of anthropogenic aerosols.

The evaluation also assessed system performance during highly dynamic, mixed-aerosol conditions and extreme events, such as the Siberian boreal wildfires of summer 2019 and the unprecedented Australian bushfires in winter 2019–2020. In these scenarios, both the MODIS and VIIRS experiments successfully tracked the rapid temporal evolution of the smoke plumes. However, both systems systematically underestimated the absolute peak AOD magnitudes. This persistent low bias is probably driven by the underlying GEOS model's ~50 km horizontal resolution used in those experiments, which smooths complex topography—altering assumed atmospheric column depths at elevated sites like Bamenda in the Cameroon highlands—and artificially dilutes highly concentrated aerosol plumes within large grid boxes. While MODIS occasionally exhibited a slight advantage in capturing peak magnitudes during rapidly evolving fires due to the extended diurnal coverage and shorter revisit

https://doi.org/10.5194/egusphere-2026-5508
Preprint. Discussion started: 29 September 2026

time of its dual-satellite constellation, the sheer volume, gapless equatorial coverage, and overlapping mid-to-high latitude retrievals of the VIIRS instrument provided highly acceptable, comparable constraints.

In conclusion, the similar spatial patterns, temporal signatures and robust statistical agreements between the MODIS and VIIRS experiments suggest that the methodology developed for MODIS translates seamlessly to the newer sensor, provided systematic training of new NNR models is performed. While subtle regional differences exist, transitioning from MODIS to VIIRS assimilation will maintain the continuity and consistency of the aerosol analysis system required for NASA's near-real-time forecasting. Furthermore, this successful implementation for NOAA-20 establishes a strong foundation for integrating future instruments in the VIIRS series, such as NOAA-21, and for eventual inclusion into multi-decadal reanalyses, though additional testing will be necessary to evaluate the simultaneous assimilation of multiple satellite observing platforms.

Code availability. GEOS is a publicly available Earth System model with source code at https://github.com/GEOS-ESM/GEOSgcm.

Data availability. All observational data used are from publicly available datasets. MODIS Collection 6.1 Level 2 aerosol products are available at https://doi.org/10.5067/MODIS/MOD04_L2.061 for Terra and https://doi.org/10.5067/MODIS/MYD04_L2.061 for Aqua. VIIRS Version 2.0 aerosol products (AERDT and AERDB) are available at https://ladsweb.modaps.eosdis.nasa.gov/missions-and-measurements/products/AERDT_L2_VIIRS_NOAA20 (last access: 31 August 2026; Lee et al., 2024; Sawyer et al., 2025). AERONET Version 3 Level 2.0 observations can be downloaded at https://aeronet.gsfc.nasa.gov/cgi-bin/webtool_aod_v3 (last access: 31 August 2026). Maritime Aerosol Network (MAN) observations can be accessed at https://aeronet.gsfc.nasa.gov/new_web/maritime_aerosol_network.html (Smirnov et al., 2009). Subsets of the Neural Network Retrieval (NNR) observational data and the GEOS model data from the assimilation experiments presented in this paper are archived at https://doi.org/10.5281/zenodo.22309153] (Buchard et al., 2026).

Author contributions. VB and PC conceived the study and led the scientific analysis. PC developed the aerosol bias correction algorithm, generated the data, and performed the analysis. VB updated the aerosol data assimilation system, conducted the assimilation experiments alongside RG, and performed the subsequent analysis. MT optimized the computational efficiency of the observation quality control. RL, VK, JL, and PG provided satellite and ground-based observations. VB and PC generated the figures and wrote the initial manuscript draft. AMdS conceived an early version of the aerosol bias correction algorithms for MODIS and provided guidance on its implementation before retiring from NASA. All authors contributed to the interpretation of the results, manuscript review and editing, and approved the final version of the manuscript.

Supplement. The supplement related to this article is available online.

Competing interests. The contact author has declared that none of the authors has any competing interests.

Acknowledgements. Simulations were performed at the NASA Center for Climate Simulation (NCCS). We thank the AERONET principal investigators and co-investigators and their staff, for establishing and maintaining the sites used in this manuscript.

References

Benedetti, A. et al., 2018, Status and future of numerical atmospheric aerosol prediction with a focus on data requirements: Atmospheric Chemistry and Physics, v. 18, p. 10615–10643, doi:10.5194/acp-18-10615-2018.

Bian, H., et al. “Source Attributions of Pollution to the Western Arctic during the NASA ARCTAS Field Campaign.” *Atmospheric Chemistry and Physics*, vol. 13, no. 9, May 2013, pp. 4707–21. *DOI.org (Crossref)*, https://doi.org/10.5194/acp-13-4707-2013.

Bloom, S. C., et al. “Data Assimilation Using Incremental Analysis Updates.” *Monthly Weather Review*, vol. 124, no. 6, June 1996, pp. 1256–71. *DOI.org (Crossref)*, https://doi.org/10.1175/1520-0493(1996)124%3C1256:DAUIAU%3E2.0.CO;2

Bocquet, M. et al., 2015, Data assimilation in atmospheric chemistry models: current status and future prospects for coupled chemistry meteorology models: Atmospheric Chemistry and Physics, v. 15, p. 5325–5358, doi:10.5194/acp-15-5325-2015.

Buchard, V., da Silva, A.M., Colarco, P.R., Darmenov, A., Randles, C.A., Govindaraju, R., Torres, O., Campbell, J., and Spurr, R., 2015, Using the OMI aerosol index and absorption aerosol optical depth to evaluate the NASA MERRA Aerosol Reanalysis: Atmospheric Chemistry and Physics, v. 15, p. 5743–5760, doi:10.5194/acp-15-5743-2015.

Buchard, V., da Silva, A.M., Randles, C.A., Colarco, P., Ferrare, R., Hair, J., Hostetler, C., Tackett, J., and Winker, D., 2016, Evaluation of the surface PM2.5 in Version 1 of the NASA MERRA Aerosol Reanalysis over the United States: Atmospheric Environment, v. 125, p. 100–111, doi:10.1016/j.atmosenv.2015.11.004.

Buchard, V. et al., 2017, The MERRA-2 Aerosol Reanalysis, 1980 Onward. Part II: Evaluation and Case Studies:, doi:10.1175/JCLI-D-16-0613.1.

Chin, M., Rood, R.B., Lin, S.-J., Müller, J.-F., and Thompson, A.M., 2000, Atmospheric sulfur cycle simulated in the global model GOCART: Model description and global properties: Journal of Geophysical Research: Atmospheres, v. 105, p. 24671–24687, doi:10.1029/2000JD900384.

Cohn, Stephen E., et al. “Assessing the Effects of Data Selection with the DAO Physical-Space Statistical Analysis System*.” Monthly Weather Review, vol. 126, no. 11, Nov. 1998, pp. 2913–26. DOI.org (Crossref), https://doi.org/10.1175/1520-0493(1998)126%3C2913:ATEODS%3E2.0.CO;2.

https://doi.org/10.5194/egusphere-2026-5508
Preprint. Discussion started: 29 September 2026

Colarco, P., da Silva, A., Chin, M., and Diehl, T., 2010, Online simulations of global aerosol distributions in the NASA GEOS-4 model and comparisons to satellite and ground-based aerosol optical depth: Journal of Geophysical Research: Atmospheres, v. 115, doi:10.1029/2009JD012820.

Collow, Allison B., et al. "Benchmarking GOCART-2G in the Goddard Earth Observing System (GEOS)." *Geoscientific Model Development*, vol. 17, no. 3, Feb. 2024, pp. 1443–68. *DOI.org (Crossref)*, https://doi.org/10.5194/gmd-17-1443-2024.

Dee, Dick P., and Arlindo M. Da Silva. "Maximum-Likelihood Estimation of Forecast and Observation Error Covariance Parameters. Part I: Methodology." *Monthly Weather Review*, vol. 127, no. 8, Aug. 1999, pp. 1822–34. *DOI.org (Crossref)*, https://doi.org/10.1175/1520-0493(1999)127%3C1822:MLEOFA%3E2.0.CO;2.

Dee, Dick P., et al. "An Adaptive Buddy Check for Observational Quality Control." *Quarterly Journal of the Royal Meteorological Society*, vol. 127, no. 577, Oct. 2001, pp. 2451–71. *DOI.org (Crossref)*, https://doi.org/10.1002/qj.49712757714.

Eck, T. F., B. N. Holben, J. S. Reid, O. Dubovik, A. Smirnov, N. T. O'Neill, I. Slutsker, and S. Kinne (1999), Wavelength dependence of the optical depth of biomass burning, urban, and desert dust aerosols, J. Geophys. Res., 104(D24), 31333–31349, doi:10.1029/1999JD900923.

Eck, T. F., et al. "Climatological Aspects of the Optical Properties of Fine/Coarse Mode Aerosol Mixtures." Journal of Geophysical Research: Atmospheres, vol. 115, no. D19, Oct. 2010, p. 2010JD014002. DOI.org (Crossref), https://doi.org/10.1029/2010JD014002.

Gelaro, Ronald, et al. "The Modern-Era Retrospective Analysis for Research and Applications, Version 2 (MERRA-2)." Journal of Climate, vol. 30, no. 14, July 2017, pp. 5419–54. DOI.org (Crossref), https://doi.org/10.1175/JCLI-D-16-0758.1.

Giglio, L., et al. "Global Estimation of Burned Area Using MODIS Active Fire Observations." *Atmospheric Chemistry and Physics*, vol. 6, no. 4, Mar. 2006, pp. 957–74. *DOI.org (Crossref)*, https://doi.org/10.5194/acp-6-957-2006.

Giles, David M., et al. "Advancements in the Aerosol Robotic Network (AERONET) Version 3 Database – Automated near-Real-Time Quality Control Algorithm with Improved Cloud Screening for Sun Photometer Aerosol Optical Depth (AOD) Measurements." Atmospheric Measurement Techniques, vol. 12, no. 1, Jan. 2019, pp. 169–209. DOI.org (Crossref), https://doi.org/10.5194/amt-12-169-2019.

Holben, B.N. et al., 1998, AERONET—A Federated Instrument Network and Data Archive for Aerosol Characterization: Remote Sensing of Environment, v. 66, p. 1–16, doi:10.1016/S0034-4257(98)00031-5.

Inness, A. et al., 2019, The CAMS reanalysis of atmospheric composition: Atmospheric Chemistry and Physics, v. 19, p. 3515–3556, doi:10.5194/acp-19-3515-2019.

Kaiser, J.C. et al., 2019, Global aerosol modeling with MADE3 (v3.0) in EMAC (based on v2.53): model description and evaluation: Geoscientific Model Development, v. 12, p. 541–579, doi:10.5194/gmd-12-541-2019.

Kaufman, YJ, Tanre, D (1996). Strategy for direct and indirect methods for correcting the aerosol effect on remote sensing: From AVHRR to EOS-MODIS. REMOTE SENSING OF ENVIRONMENT, 55(1), 65-79

Kinne, S. et al., 2006, An AeroCom initial assessment – optical properties in aerosol component modules of global models: Atmospheric Chemistry and Physics, v. 6, p. 1815–1834, doi:10.5194/acp-6-1815-2006.

https://doi.org/10.5194/egusphere-2026-5508
Preprint. Discussion started: 29 September 2026

Lary, D.J., Remer, L.A., MacNeill, D., Roscoe, B., and Paradise, S., 2009, Machine Learning and Bias Correction of MODIS Aerosol Optical Depth: IEEE Geoscience and Remote Sensing Letters, v. 6, p. 694–698, doi:10.1109/LGRS.2009.2023605.

Lee, J., Hsu, N.C., Kim, W.V., Sayer, A.M., and Tsay, S.-C., 2024, VIIRS Version 2 Deep Blue Aerosol Products: Journal of Geophysical Research: Atmospheres, v. 129, p. e2023JD040082, doi:10.1029/2023JD040082.

Levy, R.C., Mattoo, S., Munchak, L.A., Remer, L.A., Sayer, A.M., Patadia, F., and Hsu, N.C., 2013, The Collection 6 MODIS aerosol products over land and ocean: Atmospheric Measurement Techniques, v. 6, p. 2989–3034, doi:10.5194/amt-6-2989-2013.

Limpert, Eckhard, et al. "Log-Normal Distributions across the Sciences: Keys and Clues." BioScience, vol. 51, no. 5, 2001, p. 341. DOI.org (Crossref), https://doi.org/10.1641/0006-3568(2001)051%5B0341:LNDATS%5D2.0.CO;2.

Lynch, P., and Coauthors, 2016: An 11-year global gridded aerosol optical thickness reanalysis (v1.0) for atmospheric and climate sciences. Geosci. Model Dev., 9, 1489–1522, https://doi.org/10.5194/gmd-9-1489-2016.

Lucchesi, R, 2018, File Specification for GEOS-5 FP (Forward Processing): Global Modelng and Assimilation Office, https://gmao.gsfc.nasa.gov/pubs/docs/Lucchesi1203.pdf.

Mulcahy, J.P., Walters, D.N., Bellouin, N., and Milton, S.F., 2014, Impacts of increasing the aerosol complexity in the Met Office global numerical weather prediction model: Atmospheric Chemistry and Physics, v. 14, p. 4749–4778, doi:10.5194/acp-14-4749-2014.

Nowottnick, E., et al. "Online Simulations of Mineral Dust Aerosol Distributions: Comparisons to NAMMA Observations and Sensitivity to Dust Emission Parameterization." *Journal of Geophysical Research: Atmospheres*, vol. 115, no. D3, Feb. 2010, p. 2009JD012692. *DOI.org (Crossref)*, https://doi.org/10.1029/2009JD012692.

Nowottnick, E., et al. "The Fate of Saharan Dust across the Atlantic and Implications for a Central American Dust Barrier." Atmospheric Chemistry and Physics, vol. 11, no. 16, Aug. 2011, pp. 8415–31. DOI.org (Crossref), https://doi.org/10.5194/acp-11-8415-2011.

Pérez, C., Nickovic, S., Pejanovic, G., Baldasano, J.M., and Özsoy, E., 2006, Interactive dust-radiation modeling: A step to improve weather forecasts: Journal of Geophysical Research: Atmospheres, v. 111, doi:10.1029/2005JD006717.

Putman, William M., and Shian-Jiann Lin. "Finite-Volume Transport on Various Cubed-Sphere Grids." Journal of Computational Physics, vol. 227, no. 1, Nov. 2007, pp. 55–78. DOI.org (Crossref), https://doi.org/10.1016/j.jcp.2007.07.022.

Randles, C.A. et al., 2017, The MERRA-2 Aerosol Reanalysis, 1980 Onward. Part I: System Description and Data Assimilation Evaluation:, doi:10.1175/JCLI-D-16-0609.1.

Remer, L.A. et al., 2008, Global aerosol climatology from the MODIS satellite sensors: Journal of Geophysical Research: Atmospheres, v. 113, doi:10.1029/2007JD009661.

Saide, P.E., Carmichael, G.R., Liu, Z., Schwartz, C.S., Lin, H.C., da Silva, A.M., and Hyer, E., 2013, Aerosol optical depth assimilation for a size-resolved sectional model: impacts of observationally constrained, multi-wavelength and fine mode retrievals on regional scale analyses and forecasts: Atmospheric Chemistry and Physics, v. 13, p. 10425–10444, doi:10.5194/acp-13-10425-2013.

https://doi.org/10.5194/egusphere-2026-5508
Preprint. Discussion started: 29 September 2026

Sawyer, V., Levy, R.C., Mattoo, S., Cureton, G., Shi, Y., and Remer, L.A., 2020, Continuing the MODIS Dark Target Aerosol Time Series with VIIRS: Remote Sensing, v. 12, p. 308, doi:10.3390/rs12020308.

Sawyer, V., Levy, R.C., Mattoo, S., Shi, Y.R., Kim, M., Remer, L.A., and Cureton, G., 2025, An updated VIIRS dark target aerosol product for continuity with MODIS: assessing regional aerosol trends: Frontiers in Environmental Science, v. 13, doi:10.3389/fenvs.2025.1602145.

Sayer, A.M., Munchak, L.A., Hsu, N.C., Levy, R.C., Bettenhausen, C., and Jeong, M.-J., 2014, MODIS Collection 6 aerosol products: Comparison between Aqua's e-Deep Blue, Dark Target, and "merged" data sets, and usage recommendations: Journal of Geophysical Research: Atmospheres, v. 119, p. 13,965-13,989, doi:10.1002/2014JD022453.

Smirnov, A. et al., 2009, Maritime Aerosol Network as a component of Aerosol Robotic Network: Journal of Geophysical Research: Atmospheres, v. 114, doi:10.1029/2008JD011257.

Wang, H. et al., 2020, Aerosols in the E3SM Version 1: New Developments and Their Impacts on Radiative Forcing: Journal of Advances in Modeling Earth Systems, v. 12, p. e2019MS001851, doi:10.1029/2019MS001851.

Wei, S.-W. et al., 2021, The Impact of Aerosols on Satellite Radiance Data Assimilation Using NCEP Global Data Assimilation System: Atmosphere, v. 12, doi:10.3390/atmos12040432.

Xian, P. et al., 2019, Current state of the global operational aerosol multi-model ensemble: An update from the International Cooperative for Aerosol Prediction (ICAP): Quarterly Journal of the Royal Meteorological Society, v. 145, p. 176–209, doi:10.1002/qj.3497.

Zhang, J., and Reid, J.S., 2006, MODIS aerosol product analysis for data assimilation: Assessment of over-ocean level 2 aerosol optical thickness retrievals: Journal of Geophysical Research: Atmospheres, v. 111, doi:10.1029/2005JD006898.